MONOGRAFIE, STUDIA, ROZPRAWY

M37

Norbert Radek

WELDING TECHNOLOGIES IN SURFACE ENGINEERING

Kielce 2013

MONOGRAFIE, STUDIA, ROZPRAWY NR M37

Redaktor Naukowy serii
NAUKI TECHNICZNE – BUDOWA I EKSPLOATACJA MASZYN
prof. dr hab. inż. Stanisław ADAMCZAK, dr h.c.

Recenzenci:
Prof. Ing. Otakar BOKŮVKA, PhD.
Prof. dr hab. inż. Janusz KONSTANTY

Redakcja techniczna
Aneta DYNKOWSKA

Projekt okładki
Tadeusz UBERMAN

Wyd. I
Nakład: 70 egz.
Objętość: 6,0 ark. wyd.

PL ISSN 1897-2691
PL ISBN 978-83-63792-20-6

Wydawnictwo Politechniki Świętokrzyskiej
25-314 Kielce, al. Tysiąclecia Państwa Polskiego 7
tel./fax 41 34 24 581
e-mail: wydawca@tu.kielce.pl
www.tu.kielce.pl/organizacja/wydawnictwo

Contents

Foreword

Welding Technologies are considered basic techniques of manufacturing and repairs of various machine parts. Presently, they are employed in all sectors of economy. Their popularity results from the fact that they make it possible to create structures and products that have many technical and service advantages. In addition to traditional bonding and cutting of metals, welding technologies also include methods for depositing coatings and modifying the surface layer. Wide use of welding technologies depends on the manufacture of modern machines and devices employed in industries. Social and economic development, and a resultant advancement in materials engineering and electronics, has always been a driving force in the progress of welding technologies.

Surface Engineering covers all aspects of research and technical activities aimed at design, construction, reconstruction, and also investigations and applications of technological and functional surface layers that have different, i.e. better properties than the core (substrate). Those include mainly anti-abrasive, anti-corrosive, anti-fatigue, and also decorative properties. The others are optical, thermo-physical, electrical, magnetic, adhesive, ablative, bio-compatible and diffusive properties. Surface engineering is an autonomous science and technology discipline. Since 1994 it has been recognised by the Polish Committee for Scientific Research as one of the fifteen most innovative disciplines in the technology category. Surface engineering is one of manufacturing technologies (like welding, casting, also thermal, plastic and regular machining and others), in which a product of materials technology receives different surface properties.

The development of surface engineering is connected with the construction of new devices and a very complex apparatus. For those working in the field of surface engineering that means it is necessary to get continuous training to develop their expertise and skills.

The present monograph focuses on welding technologies issues in surface engineering. The material covered in the monograph is based on the results of investigations into methods that use a concentrated energy flux. Electro-spark machining, laser machining and methods of thermal spray discussed in the monograph count as welding technologies.

The material collected provides a survey, still incomplete, of current research interests in the field of welding technologies and surface engineering.

The author is convinced that the studies discussed in the monograph have been properly selected to represent the achievements of this part of the scientific community which deals with welding technologies.

I believe the present monograph can be a valuable source of information for students of mechanical engineering, young researchers, and employees of different industries who want to broaden their knowledge of welding technologies and surface engineering, or are interested in finding a solution to particular technical problems.

Norbert Radek

1. THE PROPERTIES AND APPLICATIONS OF ELECTRO-SPARK DEPOSITED COATINGS

1.1. INTRODUCTION

The origin of electrical discharge machining (EDM) dates back to 1770 when English scientist Joseph Priestly discovered the erosive effect of electrical discharges. During the 1930s, attempts were made for the first time to machine metals and diamonds with electrical discharges. Erosion was caused by intermittent arc discharges occuring in air between the tool electrode and workpiece connected to a DC power supply. These processes were not very precise due to overheating of the machining area and may be defined as "arc machining" rather than "spark machining" [1].

By controlling polarity, it is possible to remove or replace material.

The process of material removal involving erosion of the stock subjected to electric discharges is called electrical discharge machining (EDM). The surface layer forming on the product improves its operational properties [2–4].

The process of material growth resulting from electroerosion is known as electro-spark alloying (ESA) or electro-spark deposition (ESD). The erosion of the anode and the spark discharges between the electrodes result in the formation of a surface layer with properties different from those of the base material [5, 6].

Electro-spark alloying is one of the methods that require concentrated energy flux. The method was first used in the USSR in the 1940s almost simultaneously with the destructive electrical discharge machining. The ESA technique was studied intensively in the 1960s. In the next decade, it was commonly applied to deposit hard-melting materials on selected metals and alloys, mainly steel. Polish scientists became interested in electro-spark alloying of coatings as early as in the 1980s.

Electro-spark deposition (ESD) is a cheap high-energy process. Developed in the post-war period, the technology has been frequently modified. Its main advantages are the ability to select precisely the area to be modified, the ability to select the coating thickness, which may range from several to several dozen micrometers, good adhesion of a coating to the substrate, and finally, inexpensive and simple equipment for coating deposition.

The processes of coating formation on metal parts including electro-spark deposition involve mass and energy transport accompanied by chemical, electrochemical and electrothermal reactions [7]. Today, different electro-spark deposition techniques are used; they are suitable for coating formation and surface microgeometry formation [8, 9].

Coatings produced by electro-spark deposition are applied:

- to protect new elements
- to recover the properties of worn elements.

Electro-spark alloying is becoming more and more popular as a surface processing technology. Electro-spark deposited coatings are frequently applied in

industry, for example, to produce implants or cutting tool inserts. The coatings are deposited with manually operated equipment or robotized systems.

Research on this technology is being conducted all over the world, and the companies interested in applying it include NASA and the US Navy [10, 11].

As electro-spark coatings are reported to be resistant to wear and corrosion, they can be applied, for instance, to:

- ship propeller components
- casting moulds
- fuel supply system components
- exhaust system components.

The electro-spark deposition coating is characterized by a non-etching structure. The surface layer is constituted in environment of local high temperature and high pressure. Electro-machining is characterised by [2]:

- shock wave pressure coming from electric spark is $(2–7)\cdot 10^3$ GPa
- temperature riching $(5–40)\cdot 10^3$°C.

The EDS process is depicted schematically in Figure 1.1.

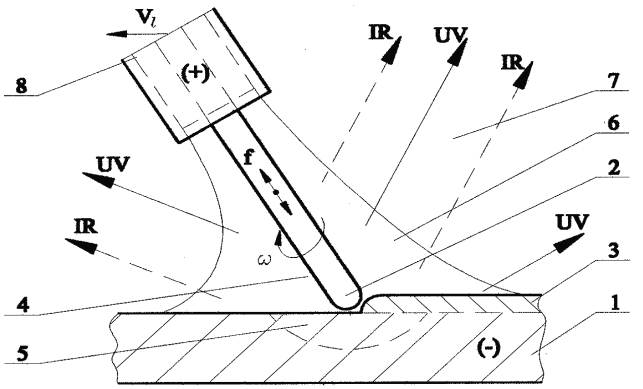

Fig. 1.1. *Scheme of surface layer forming by electro-spark deposition method: 1 – material of base (cathode), 2 – working electrode (anode), 3 – created coating with established operational features, 4 – plasma, 5 – diffusive or reactive-diffusive zone, 6 – nearer surrounding (shielding gas), 7 – further surrounding (air), 8 – electrode holder with channels supplying gas, IR – infrared radiation, UV ultraviolet radiation [7]*

1.2. PHYSICAL BASICS OF ELECTRO-SPARK ALLOYING

Since 1946, when B.R. Lazarenko and N.I. Lazarenko patented electro-spark machining of materials [12], the investigations into the physics of electric erosion of materials in removal machining (EDM – Electro Discharge Machining) and increment machining (ESA – Electro-Spark Alloying) have been conducted by research teams all over the world.

According to refs [13, 14], the occurrence of three areas is characteristic of the erosion process caused by an electric discharge:

– area adjacent to the anode
– discharge channel (presently termed a plasma channel)
– area adjacent to the cathode.

B.N. Zolotych [14] claims that in order to learn about the processes of electric erosion, it is necessary to specify the mechanism of transfer of energy delivered in a pulse to the areas directly participating in the discharge process, namely electrodes, dielectric liquid or gases. The energy causes erosion of electrodes. The character of energy transfer to the anode and the cathode is different and depends mainly on the current carriers. On the anode, the whole current is carried by electrons, whereas on the cathode, it is carried by ions and electrons. As a result of the model of electric discharge adopted by B.N. Zolotych, the processes on the anode and on the cathode are considered separately.

The energy of a pulse can be expressed as follows [14]:

$$W_i = \int_0^{t_i} U(t)I(t)dt \tag{1.1}$$

where: W_i – pulse energy, $U(t)$ – pulse voltage as a function of time, $I(t)$ – pulse current intensity as a function of time, t_i – pulse duration.

The energy of a pulse, in its simplified form, can be calculated from the dependence [14]:

$$W_i = U_r \cdot I_r \cdot t_i \tag{1.2}$$

where: W_i – pulse energy, U_r – amplitude of the working voltage, I_r – amplitude of the intensity of the working current, t_i – pulse duration.

The energy supplied to the electrode (anode and cathode) surfaces in the electro-spark alloying is written by B.N. Zolotych [14] as a sum:

$$W_E = W_A + W_K \tag{1.3}$$

where: W_E – energy transferred to the electrodes, W_A – energy transferred to the anode, W_K – energy transferred to the cathode.

In turn, the energy of the pulse [14] can be presented as follows:

$$W_i = W_E + W_W \tag{1.4}$$

where: W_i – pulse energy, W_E – energy transferred to the electrodes, W_W – energy acting in the discharge channel.

Energy transfer to the electrodes can be achieved by means of the following processes [2, 14, 15]:

– the cathode bombardment by ions due to the action of the electric field in the zones adjacent to the electrodes and the anode bombardment by electrons;
– the discharge channel radiation;
– thermal, i.e. gas kinetic bombardment by particles contained in the discharge channel;
– for small thicknesses of the gap between the electrodes, energy transfer between the electrodes can proceed because of the action of vapour streams produced on the anode and the cathode.

Electro-spark alloying can be applied to all the materials that are current conductors regardless of their hardness, shape or toughness [16].

1.2.1. Polarity of electrodes

The polarity of electrodes decides about the character of the machining process, whether it is removal machining (EDM) or increment machining (ESA). The concept was used for the first time by B.R. Lazarenko [17], and defined by B.N. Zolotych in work [14]. According to B.R. Lazarenko [17], the polarity effect depended on the melting point of the electrodes, but B.N. Zolotych [14] demonstrated that it also depended on the pulse energy and pulse discharge time.

In electro-spark alloying, the eroded material is transferred from the anode to the cathode, and consequently a coating is formed on the cathode surface. The coating consists of either pure anode material or results from the interaction of the materials of the electrodes and the interelectrode medium which is usually air. The intensity of the process of the material transfer depends on many factors [6].

An important factor that influences the effect of polar transfer of the material is the phenomenon of simultaneous erosion of the anode and the cathode. This effect is expressed by the polarisation coefficient K_n [15, 19]:

$$K_n = \frac{\gamma_k}{\gamma_a} \tag{1.5}$$

where: K_n – polarisation coefficient, γ_k – cathode erosion [g], γ_a – anode erosion [g].

For the case when $K_n < 1$, the transfer of the material occurs (positive polarity), if $K_n > 1$ the transfer of the material virtually does not take place (negative polarity).

The following conditions are true for a majority of electrodes:
– if $(T_t)_k \geq (T_t)_a$, $K_n < 1$
– if $(T_t)_k \leq (T_t)_a$, $K_n > 1$

where: $(T_t)_a$ – anode melting point, $(T_t)_k$ – cathode melting point.

The polarisation coefficient K_n depends on the pulse discharge time and energy, and for electrodes made of the same materials, on their thermal conductivity.

According to the author of work [15], the polarisation coefficient can be expressed as follows:

$$K_n = \frac{Q_k(k,t_i,W_i)\cdot\psi_a(T_t,c,q_t)}{Q_a(k,t_i,W_i)\cdot\psi_k(T_t,c,q_t)} \tag{1.6}$$

where: K_n – polarisation coefficient, $Q_{k,a}$ – amount of heat released on the cathode and the anode, $\psi_{k,a}$ – total heat of the phase change of both electrodes, k – thermal conductivity, W_i – pulse energy, t_i – pulse duration, T_t – electrode melting point, c – electrode heat capacity, q_t – electrode heat of fusion.

The above dependence on polarisation coefficient K_n takes into account basic thermal processes that proceed in the discharge channel and on the surface of electrodes.

In work [19], the author demonstrated that for K_n much higher than unity, the transfer of the material to the cathode takes place, but simultaneously the cathode mass decrement occurs.

According to works [19, 20], the polar transfer of mass is affected by the properties of the gaseous environment, in which the electric erosion process takes place. Other factors that influence the transfer include the size of the interelectrode gap and changes in the properties of electrode surfaces when those interact in the pulse discharge [15, 21].

1.3. EXPERIMENTAL

Coatings were deposited on the C45 grade plain-carbon steel by the ESD method using a portable EIL-8A electro-spark deposition facility (TRIZ, Ukraine). Electrodes containing 85% WC, 10% Co and 5% Al_2O_3, were produced using the powder metallurgy hot pressing route [22]. The main characteristics of powders used in this work are included in Table 1.1.

Table 1.1. *Powders used to manufacture electrodes*

Powder	Particle size, μm	Producer
WC	~0.2	OMG
Co	~1.4	Umicore
Al_2O_3	18÷60	Sulcer-Metco

The powders were mixed for 30 minutes in the chaotic motion Turbula T2C mixer. The mixture was then poured into rectangular cavities of a graphite mould, each 6 × 40 mm in cross section, and consolidated by passing an electric current through the mould under uniaxial compressive load. A 3 minute hold at 950°C and

under a pressure of 40 MPa permitted obtaining electrodes of porosity <10% and strength sufficient to maintain integrity when installed in the electrode holder.

The equipment used for electro-spark alloying was an EIL-8A model. Basing on the results of previous research as well as instructions given by the producer, the following parameters were assumed to be optimal for ESA:

- voltage, $U = 230$ V
- capacitor volume, $C = 150$ μF
- current intensity, $I = 2.4$ A.

The electro-spark deposition equipment is illustrated in Figure 1.2.

Fig. 1.2. *EIL-8A electro-spark deposition – equipment*

The quality of electro-spark deposition depends mainly on the shape, duration, and average value of current or pulse power. An average value of current is directly proportional to the number of generators operating in parallel. Figure 1.3 shows a schematic diagram of a single pulse generator and Figure 1.4 presents shape of a current impulse from this device.

Electrical energy stored in capacitor C2 is transmitted to the circuit: substrate – electrode in the form of a spark discharge and current flow. The process is initiated by switching on/off a transistor Q1. The switching frequency of the transistor is of the order of several to several dozens kHz. The capacitor C1 allows changing the shape and duration of an impulse as well as affecting the pulse-duty while setting pulse frequency of transistor Q1.

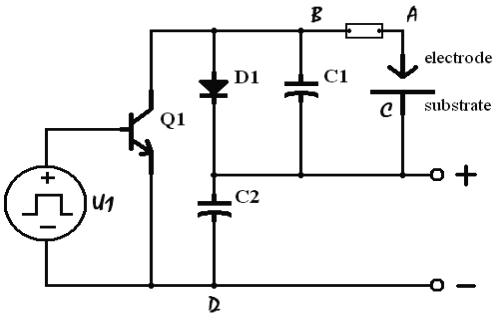

Fig. 1.3. *Schematic diagram of a single pulse generator*

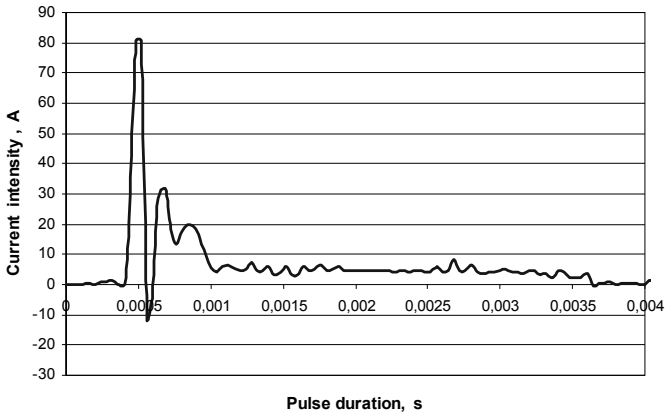

Fig. 1.4. *Shape of a current impulse*

1.4. RESULTS AND DISCUSSION

1.4.1. Microstructure and X-ray diffraction analysis

A characteristic feature of any electro-spark deposited coating is that the new layer has a difficult-to-etch structure, i.e. it remains white. Similar layers are produced by grinding and lapping. What the processes have in common is high temperature and high loads applied locally. Electro-spark deposition differs from grinding and lapping in the process intensity: the pressure of the shock wave from an electric spark discharge is $(2–7)\cdot 10^6$ N/mm^2 and the temperature reaches values of the order of $(5–40)\cdot 10^3$°C (in grinding it does not exceed 1000°C).

The temperature during an electro-spark discharge increases locally and it is much higher than the boiling point of the materials the electrodes are made of.

A high heat transfer rate causes the temperature within the layer to fall rapidly to the solidifying point, the thickness of the coating being of the order of several micrometers. The processes of crystallization, phase transition and chemical interaction occur in the solid phase. Electro-spark deposited coatings are fine-grain non-equilibrium structures, which are heterogeneous in composition, microstructure and properties. They are characterized by very high adhesion to the underlying substrate as a result of diffusion or reactive diffusion processes.

A microstructure analysis was conducted for WC-Co-Al_2O_3 coatings using the Joel JSM-5400 scanning electron microscope and the Neophot 2 light microscope.

In Figure 1.5 the microstructure of an ESD WC-Co-Al_2O_3 coating is illustrated. It is clear that the thickness of the obtained layers was from 60 to 70 μm, whereas the heat affected zone (HAZ) ranged approximately from 30 to 40 μm into the substrate. Figure 1.5 also reveals a clear boundary between the coating and the substrate, pores and microcracks.

A Philips PW 1830 X-ray diffractometer with CuKα radiation, operating at 40 kV and 30 mA, was used for phase(s) identification. As shown in Figure 1.6, the superficial layer of the coating consists of WC and W_2C as well as a small amount

of Co_2C and Al_2O_3. W_2C is known to appear as an intermediate during the formation and dissolution of WC. Besides, it has been found that peaks from the W_2C phase are most intense.

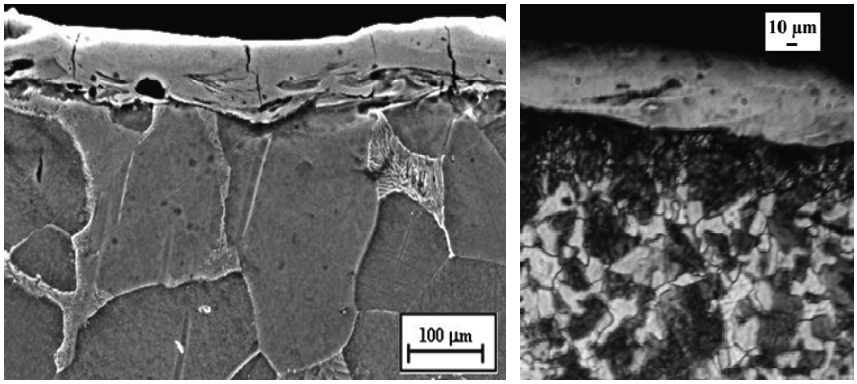

Fig. 1.5. *SEM (left) and LM (right) micrographs of the polished cross section throug a WC-Co-Al_2O_3 ESD coating on C45 steel substrate*

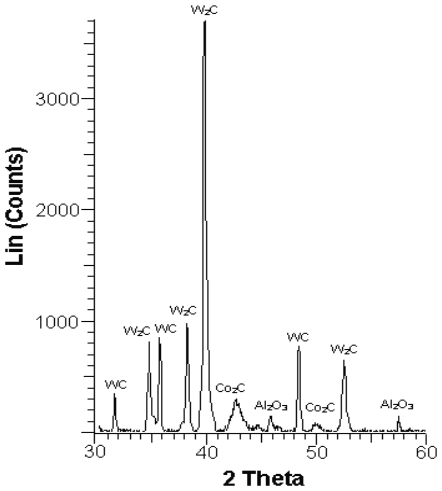

Fig. 1.6. *X-ray diffraction pattern of the WC-Co-Al_2O_3 coating*

1.4.2. Microgeometry measurements

One of the main disadvantages of the coatings produced by electro-spark alloying is high surface roughness. By reviewing the literature and analyzing the latest developments in this technology, one can notice that the surface generation process involves erosion of the base material and formation of microcraters and ridges by particles leaving the electrode. The surface is regular with rounded microroughness peaks. The effect of the process parameters on the formation of surface roughness has been described in numerous publications. By controlling

these parameters, it is possible to obtain surfaces with pre-determined microgeometry. Electro-spark alloying allows producing surfaces with enhanced roughness called surface relief.

The roughness of the WC-Co-Al_2O_3 coatings was measured at the Laboratory for Measurement of Geometric Quantities of the Kielce University of Technology using a TALYSURF CCI equipment.

The roughness was measured in two directions perpendicular to each other. Then, the average value was calculated: Ra = 4.99÷5.66 μm.

The without coatings steel specimens (C45) had a roughness from 0.46 to 0.53 μm.

Figure 1.7 presents an example three dimensional surface microgeometry measurement of the WC-Co-Al_2O_3 coatings.

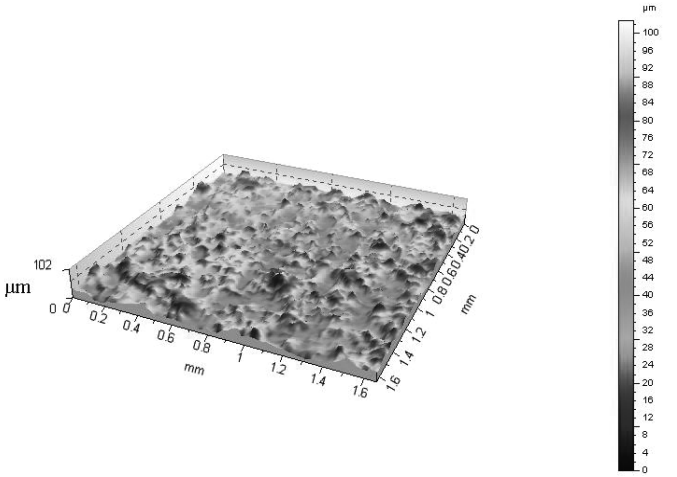

Fig. 1.7. *Three dimensional surface microgeometry of the WC-Co-Al_2O_3 coating deposited*

1.4.3. Microhardness and adhesion tests

The microhardness of the specimens with WC-Co-Al_2O_3 coatings was analyzed applying a load of 0.4 N and using the Vickers method. The indentations were made consecutively in three zones: the coating, the heat affected zone (HAZ) and the base material. The results are given in Table 1.2.

Table 1.2. *Results of the microhardness tests for the WC-Co-Al_2O_3 coating*

Measured zones	Microhardness HV0.4			Mean value HV0.4
	Measurement number			
	1	2	3	
Coating	877	931	911	906
HAZ	391	388	372	384
Substrate	270	288	279	279

The average microhardness of the base material after ESA was 279 HV0.4. The value was the same as that at the initial state. The average microhardness of the WC-Co-Al_2O_3 coating was 906 HV0.4. Thus, there was a 225 percent increase compared to that of the base material. The microhardness of the heat affected zone after electro-spark alloying was 38% higher in relation to that of the base material.

A scratch test was conducted to test adhesion of the WC-Co-Al_2O_3 coatings. Adhesion tests were conducted using REVETEST instrument (CSEM, Switzerland). The diagram showing the operation of the tester is presented in Figure 1.8. The measurements were performed at a load increase rate of 103.2 N/min, a table feed rate of 9.77 mm/min and a scratch length of 9.5 mm.

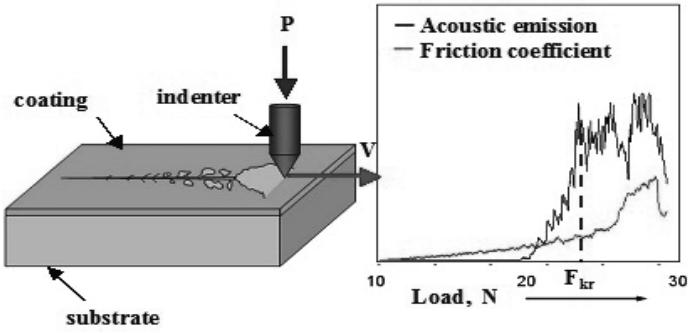

Fig. 1.8. *Diagram of the stand for scratch tests of coating adhesion together with an idealized graph used to indicate the value of the critical force on the basis of the profile of acoustic emission signal and the friction force*

A special Rockwell diamond cone indenter with a corner radius of 200 μm, was used to scratch the samples at a gradually increasing normal load. The information about the cracking or peeling of layers was obtained basing on the measurements of the material resistance (tangential force) and the registration of acoustic emission signals. The lowest normal force causing a loss of adhesion of the coating to the substrate is called a critical force and is assumed to be the measure of adhesion.

The critical force was determined basing on the records of changes in the acoustic emission signals and the tangential force as well as on the results of observations with an optical microscope fitted in the REVETEST tester. The values of the critical force were established by comparing the scratches left by the indenter with the responses of acoustic emission signals. Table 1.3 shows the values of the critical force obtained from three measurements on a given sample, the mean force values and standard deviations. The mean value of the critical force calculated from three measurements performed on the WC-Co-Al_2O_3 coating was 7.64 N.

Measurements with PG-2/200 shape analyser made it possible to observe transverse profile of scratches in the examined coatings. An image of a scratched specimen is shown in Figure 1.9. Observations indicate that the coating scratching with diamond probe is accompanied by plastic deformation of the substrate. It can

be evidenced by substantial material pile-up along the groove drawn. As a result of plastic deformation, a furrow (wave) of deformed material is formed in front of the moving indenter. In accordance with the author's observations, and also tests described by Hebda [23] and Kupczyk [24], the height of the deformed material depends on the material yield strength. The lower is the yield strength, the greater is the wave height.

Table 1.3. *Results of the adhesion test*

Coating	Critical force, N			Mean value, N
	Measurement number			
	1	2	3	
WC-Co-Al_2O_3	8.65	7.94	6.32	7.64

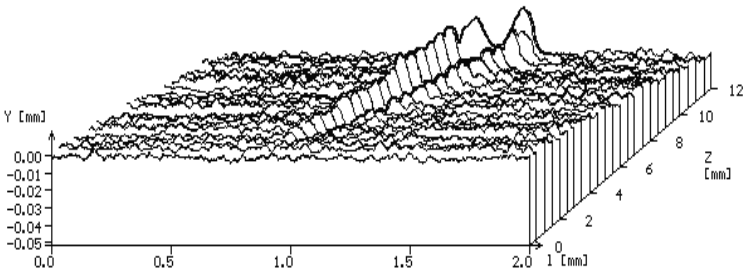

Fig. 1.9. *Spatial image of the scratched WC-Co-Al_2O_3 coating*

1.4.4. Corrosion resistance tests

The corrosion resistance of the WC-Co-Al_2O_3 coatings and the underlying substrate was analyzed using a computerized system for electrochemical tests, Atlas'99, produced by Atlas-Sollich. The potentiodynamic method was applied, because it is reported to be one of the most effective methods of electrochemical testing.

The cathode polarization curve and the anode polarization curve were determined by polarizing the samples with a potential shift rate of 0.2 mV/s in the range of ±200 mV of the corrosive potential, and with 0.4 mV/s in the range of higher potentials. Samples with a marked area of 10 mm in diameter were polarized up to a potential of 800 mV. The polarization curves were drawn for samples exposed for 24 hours to a 3.5% NaCl solution so that the corrosive potential could be established. The tests were performed at 21 ±1°C.

The results are summarised in Table 1.4. A diagram of the three-electrode chamber for electrochemical corrosion testing is presented in Figure 1.10.

Table 1.4. *Corrosion current densities of the tested materials*

Material	Corrosion current density (I_k), μA/cm^2
C45	35.4
WC-Co-Al_2O_3	16.8

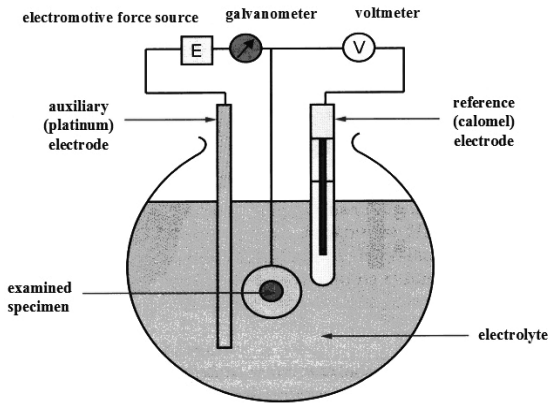

Fig. 1.10. *Schematic view of three-electrode chamber used in corrosion resistance tests [25]*

The WC-Co-Al_2O_3 coating was reported to have the highest corrosion resistance. The corrosion current density of the coating was 16.8 μA/cm^2, while that of the C45 steel substrate was 35.4 μA/cm^2. Applying the WC-Co-Al_2O coating improved the sample corrosion resistance by approx 100%. The fusion of the coating and the substrate resulted in a considerable heterogeneity of electrochemical potentials on the coating surface. The microcracks in the surface layer also contributed to intensification of the corrosion processes.

1.4.5. Wear resistance of beaters

In the experiment, the coatings were electro-spark deposited on hammer faces made of carbon steel C45 (Fig. 1.11) – the cathode – using a WC-Co-Al_2O_3 electrode.

Sixteen specimens were tested: eight with electro-spark deposited WC-Co-Al_2O_3 coatings and eight uncoated ones.

Fig. 1.11. *Working surface of unworn specimen before deposition of WC-Co-Al_2O_3 coating*

All specimens were weighed for the first time before the tests. Then, eight of them were coated with WC-Co-Al_2O_3 and weighed again. It should be noted that only the working surfaces were strengthened. The next stage involved mounting the beaters in a hammer mill operating in Nordiska Ekofiber Polska Ltd. (Fig. 1.12). The eighteen beaters were placed symmetrically along the mill shaft. After 250 hours of operation, all of them were weighed again. The data are shown in Tables 1.5 and 1.6.

Table 1.5. *Mass of the beaters with WC-Co-Al_2O_3 coatings*

Specimen number	Measurement number			Mass loss
	I [g]	II [g]	III [g]	[g]
1 N	936.43	936.49	936.31	0.18
2 N	947.62	947.66	947.43	0.23
3 N	969.13	969.15	969.03	0.12
4 N	949.87	949.92	949.71	0.21
5 N	937.69	937.71	937.47	0.24
6 N	929.75	929.79	929.64	0.15
7 N	958.32	958.37	958.21	0.16
8 N	967.28	967.32	967.11	0.21
			average value	**0.19**

Table 1.6. *Mass of the beaters without coatings*

Specimen number	Measurement number		Mass loss
	I [g]	II [g]	[g]
1 W	937.72	937.48	0.24
2 W	934.19	933.54	0.65
3 W	948.86	948.64	0.22
4 W	965.72	965.29	0.43
5 W	953.78	953.31	0.47
6 W	943.33	942.89	0.44
7 W	921.18	920.45	0.73
8 W	972.83	972.62	0.21
		average value	**0.42**

Table 1.5 presents measurement results for the specimens with WC-Co-Al_2O_3 coatings. Column I shows the mass of the beaters before electro-spark alloying; in

column II we have the mass of the beaters with electro-spark deposited WC-Co-Al_2O_3 coatings, and in column III the mass of the beaters after 250 h of operation in the mill. Table 1.6 contains results for the uncoated specimens before use (column I), and after 250 hours of operation in the mill (column II).

The mass loss analysis showed that the beaters with the WC-Co-Al_2O_3 coatings had a lower wear rate than the uncoated beaters. The latter are predicted to operate for approximately 2–3 years. The investigations will be continued as there is not enough data confirming that the application of WC-Co-Al_2O_3 coatings improves the long-term wear resistance of beaters.

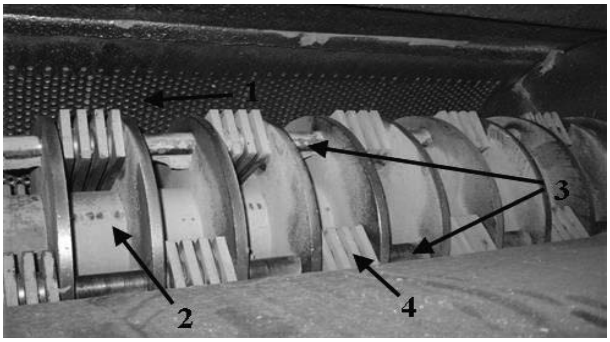

Fig. 1.12. *A view of the inside of the mill for waste paper grinding: 1 – sieve, 2 – main shaft, 3 – fixing pivots, 4 – beaters*

1.4.6. Electric pulse measurements

Electric pulses of the electro-spark alloying are generated in the system presented in Figure 1.13.

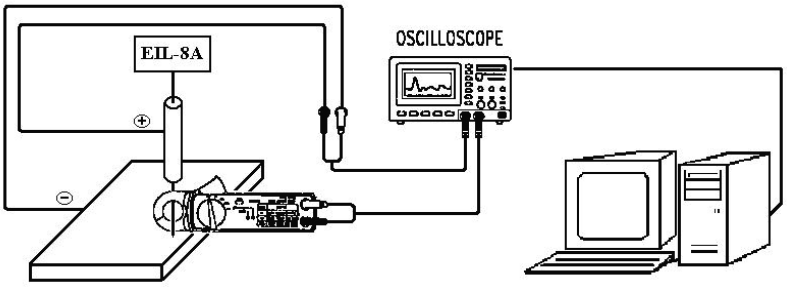

Fig. 1.13. *The measurement system [26]*

While conducting investigations into the process of electro-spark alloying, it is necessary to take measurements of the current intensity and the power of electric pulses used. Transistor pulse generation system is energised from the power source, which is a power capacitor. The way of taking measurements is presented in Figure 1.13.

For current measurements, a CM-05 digital probe by Prova Instruments Inc. was employed. The probe, which has jaws, is current-to-voltage transducer based on a Hall sensor. The probe measures AC/DC current in the bar and ensures that the measuring and high current systems are galvanically separated. The probe voltage output signal is fed directly to the TDS 210 digital oscilloscope (Tektronix). In the other channel of the oscilloscope, the voltage between the electrode and the machined workpiece is measured. The measurement data are transferred to the computer via TDSCM communications module. Measured quantities are also available as a file in ASCII format.

In order to determine the patterns of current and voltage of electric discharge in the ESA process, a measurement stand comprising Hewlett-Packard 54602A digital oscilloscope, current probe and IBM PC was used. The stand makes it possible to record instantaneous values of the current and spark discharge voltage. Digital oscilloscope accounts for simultaneous measurements of voltage and current. Buffer memory allows remembering 500 samples, which makes it possible to record a few discharge cycles (at appropriately selected time base). 8-bit resolution of the amplitude measurements may seem too low, yet the results obtained are satisfactory. The system suffers from a minor drawback due to the fact that it is possible to record only two patterns. The parameters of the process of electro-spark alloying were selected experimentally.

Exemplary patterns of current and electric discharge voltage recorded in electro-spark alloying are presented in graphs (Figs. 1.14 and 1.15).

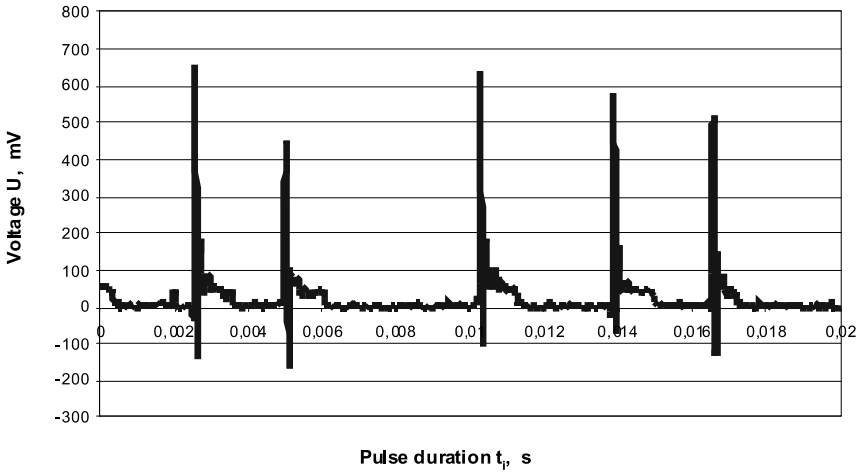

Fig. 1.14. *Pattern of changes in voltage parameters (I = 0.4 A; C = 150 μF)*

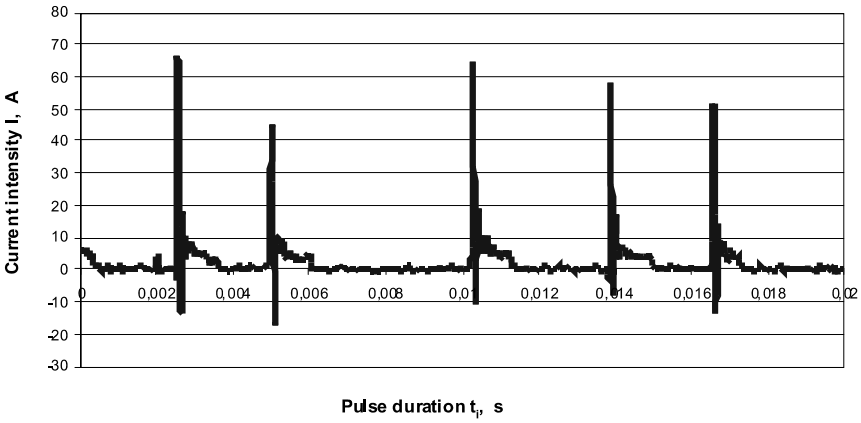

Fig. 1.15. *Pattern of changes in current parameters (I = 0.4 A; C = 150 μF)*

Basic electric quantities in a discharge, i.e. current $i(t)$ and voltage $u(t)$ of an electric pulse can be read form the graphs. After digital processing of those quantities, it is possible to compute, e.g. instantaneous power of an electricd pulse, which is expressed by formula $p(t) = u(t) \cdot i(t)$. Additionally, the duration of the spark discharge pulse can be read. If current, voltage and the duration of the spark discharge pulse are given, an instantaneous energy of an electric pulse can be calculated. From the literature, it is known that the thickness of the deposited coating and its functional properties are influenced to the greatest extent by the pulse energy. The current and voltage characteristics obtained could be used to optimise the ESA process, so that the coatings with desirable functional properties could be designed.

Conclusions:

The following conclusions can be drawn from the analysis and test results.

1. The microstructure analysis revealed that the coating thickness was 60–70 μm, whereas the heat affected zone ranged approximately 30–40 μm. The coatings possessed microcracks and pores.
2. A significant increase in roughness Ra was reported for specimens with WC-Co-Al_2O_3 coatings. Higher roughness, however, is not always considered a disadvantage. Under certain circumstances, valleys in the roughness profile act as lubricant reservoirs, which increases the rate of heat transfer and that of catalysis.
3. The microhardness of the WC-Co-Al_2O_3 coating produced by electro-spark alloying was 906 HV0.4, while that of the base material – C45 steel – was 279 HV0.4.
4. The mean value of the critical force of the WC-Co-Al_2O_3 coating calculated from three measurements was 7.64 N.

5. The obtained I_k values indicate over 100% increase in corrosion resistance of the ESD coated sample compared to uncoated C45 steel substrate.
6. The coating surface is composed of WC and W_2C besides a small amount of Co_2C and Al_2O_3.
7. The durability of beaters was studied under real conditions; the specimens with WC-Co-Al_2O_3 coatings were reported to be more wear resistant than the uncoated ones.

Further research will be targeted at determining the long-term wear resistance of beaters with WC-Co-SiC and TiB_2-Co-Al_2O_3 coatings produced by electro-spark alloying.

The measurement system that was constructed includes: the EIL-8A device, the TDS 210 digital oscilloscope (Tektronix) and CM-05 digital probe. The system makes it possible to take measurements of the basic electric quantities, i.e. current $i(t)$ and voltage $u(t)$ of an electric pulse. The system can also digitally process those quantities, which includes determining additional electric quantities, e.g. instantaneous power of an electric pulse $p(t) = u(t) \cdot i(t)$.

The shortcoming of the measurement system used consists in the recording of only two patters, and also a relatively slow data transmission from the oscilloscope to the computer. Additionally, digital oscilloscope employed for measurements is based on 8-bit convertors, which diminishes measurement accuracy. An alternative solution is to replace the oscilloscope with a multi-channel 14-bit control-measurement card. Due to FIFO buffer or DMA channel, it ensures high speed and accuracy of A/D processing.

2. THE SURFACE GEOMETRIC STRUCTURE AND TRIBOLOGICAL PROPERTIES OF THE ELECTRO-SPARK DEPOSITED WC-Cu COATINGS BEFORE AND AFTER LASER TREATMENT

2.1. ESD AND LBM – MODIFICATION METHODS

There are many methods for producing surface coatings, such as electroplating and plasma spraying. Very thin layers can be deposited by vapour deposition. Various surface treatment techniques have been developed to improve the desired properties of the deposited layers. Some of these methods are expensive and should be used only for unique applications, where the high cost is justified. However, for most applications, there is a need for low cost coatings of good properties. This study is an attempt to improve a widely used low cost method of electro-spark deposition (ESD). It has been already recognized as an economically effective surface coating [27–29]. ESD is also widely used for its relative low cost equipment required for this process. The deposition of the coating is achieved by an electrical circuit, which generates sparks between the electrode and the work-piece. Electrical pulses of high frequency and high direct current between the electrode (anode) and work-piece (cathode) release very hot micro-particles of electrode material, resulting in continuous micro-welding coating on the work-piece surface. Important advantage is that the coating is bonded with relatively low heat. This energy saving is because only the micro particles are heated, while the body of the work-piece remains at low temperature. ESD has been known by several other terms such as spark hardening, electric spark toughening, and electro-spark alloying (ESA).

Electro-spark deposited coatings have some disadvantages but these can be easily eliminated. One of the methods is laser beam machining (LBM); a laser beam is used for surface polishing, surface geometry formation, surface sealing or for homogenizing the chemical composition of the deposited coatings [30–33].

It is envisaged that the advantages of laser-treated electro-spark coatings will include:

- lower roughness
- lower porosity
- better adhesion to the substrate
- higher wear and seizure resistance
- higher fatigue strength due to the occurrence of compressive stresses on the surface
- higher resistance to corrosion.

The work discusses the properties of electro-spark deposited WC-Cu coatings subjected to laser treatment. The properties of the coatings after laser treatment were assessed by means of: microstructure and X-ray diffraction analysis, surface geometric structure and roughness measurement, microhardness tests and tribological studies.

2.2. PHYSICAL PROCESSES THAT OCCUR IN LASER BEAM MACHINING OF ELECTRO-SPARK COATINGS

In laser machining of electro-spark coatings the following can occur most frequently:

1. With a high-melting coating, the substrate melts and the coating does not.
2. Only the coating melts.
3. Both the coating and the substrate melt.
4. The coating is vaporised and plasma is generated.

Thermal conductivity (k) is an important parameter that decides about the thermal effects in laser beam machining of electro-spark coatings. The literature on the subject [34] states that 90% of the energy absorbed by the material due to the action of a laser beam is transferred into the material by means of thermal conduction and approx. 10% is radiated through the surface layer.

In the diagram of a laser beam action on the electro-spark coating, which is presented below (Fig. 2.1), coating, diffusion and the substrate material zones can be differentiated. Each zone has different thermal conductivity ($k_1 \neq k_2 \neq k_3$). The values of k primarily depend on the materials of the coating and the substrate that are used. In laser treatment of electro-spark coatings, thermal resistances on the concrete – substrate boundary do not occur because the diffusion link between the two zones does not hamper the heat transfer.

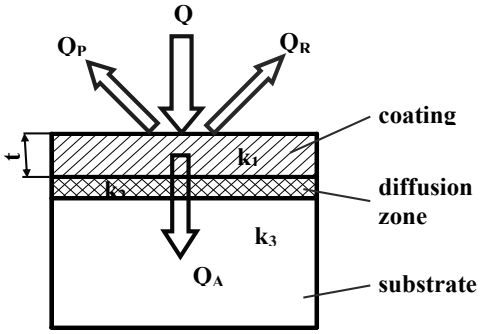

Fig. 2.1. *Diagram of laser beam action on the electro spark coatings: k_1, k_2, k_3 – thermal conductivities, t – coating thickness, Q – total power of laser-emitted radiation, Q_A – total power absorbed by the material, Q_R – total power reflected by the material surface, Q_P – total power transferred by radiation*

The carrying away of the heat is low for thin coatings (it depends mainly on thermal conductivity), as a result, after a laser exposure, the site affected by a laser beam may remain liquid [35, 36]. For higher coating thicknesses, the melted area dwindles (crystallisation occurs) already during the action of a laser beam when the volume of the unmelted material is seven times greater than the volume of the melted material [37]. The phenomena mentioned above should be experimentally validated for laser treatment of electro-spark coatings 8–60 μm thick.

Non-uniform thickness of coatings can influence the effects of laser treatment to a large extent. For the same power density, different effects may be produced at different sites of the treated coating, including disadvantageous ones, e.g. the coating vaporisation.

When the meting point of the layers deposited by electro spark treatment (e.g. WC, TiB_2, Mo, Ti) is higher than that of the steel substrate (e.g. C45 steel), it is possible that local partial meltings of the substrate under the unmelted layer will occur. After solidification, columnar or equiaxial (depending on the rate of cooling) crystals are formed, orientated along the heat transfer direction. Also, martensitic and bainitic structures, and fine-grained phases and compounds are formed.

With appropriately selected parameters of laser treatment, melting proceeds only in the electrospark coating. For coatings that have high thermal conductivity (e.g. copper), the solidification of the molten metal area starts when the laser beam is operating, because of heat being intensively carried away into the material. As regards metal coatings that have low thermal conductivity (e.g. Al_2O_3) heat transfer is slow, thus the solidification of the molten metal will take longer. On the surface of laser irradiated materials that have low thermal conductivity vaporisation begins before the impulse intensity reaches the maximum value, which may lead to the vaporisation of a thin coat.

The melting of an electro-spark coating results in an increase of its density, which leads to reduced porosity and elimination of surface defects, such as hairline cracks, delamination, cracks or open pores. In some cases the smoothing of the surface may occur.

At very high rates of cooling, the viscosity of the liquid metal increases so much that crystallisation nuclei are not able to form. The molten metal does not crystallise but it solidifies in a disordered manner forming an amorphous layer. Such layers can, among others, form metal – refractory metal compounds (e.g. Cu, Co, Fe with WC, Al_2O_3, TiB_2).

Laser beam melting of an electro spark coating deposited on the steel substrate can cause simultaneous melting and mixing of both materials (laser alloying). The action of the laser beam melts the materials. The molten pool of the materials is formed, in which they mix together vigorously, because of convective and gravitational motion and the pressure of the laser beam. The melting process starts at the coat and spreads (through convection and conduction) to the sub-surface layer of the substrate. In addition, the alloying material (coating) entirely dissolves in the substrate material. A diffusion zone is formed on the boundary of the solid state and the liquid state. After the action of the beam stops, the alloy solidifies and the substrate material in the neighbourhood of the alloy becomes hardened.

In deep melting of the thin coating by a laser beam, the coating vaporisation and plasma generation often occur when the power density exceeds 10^7 W/cm^2. Metal vapours and plasma acting on the molten metal produce different physical processes than it is the case when no vapours are present. A pit is formed in the liquid metal at the site of the laser beam penetration into the material due to the pressure exerted by the vapour. This process is disregarded in the models of thin

layer melting, even though the action of vapours can significantly affect the shape of the surface after solidification. Vapour, among others, cools the molten material, which accelerates its solidification. Vaporisation and plasma generation phenomena are undesirable in laser treatment of thin electro spark coatings because the coating will be removed or damaged, which will affect the service properties of the technological surface layer. Such phenomena are eliminated by appropriately selecting the parameters of the treatment.

The action of the shock laser (power density up to 10^8–10^{10} W/cm^2) on a thin coating can cause changes in the structure of the coating and the substrate material, fracture or bursting of the coating and its rapid vaporisation accompanied by plasma generation. A major advantage of the shock laser, which employs both shock wave energy and a mechanical impulse, is the occurrence of compressive stresses in the top layer and the elimination of micro-cracks. A disadvantage involves the formation of a crater, and thus deterioration of the quality of the surface irradiated with the laser.

In the surface engineering, a laser beam can be used for ablation, often treated as vaporisation. The ablation process takes place due to the impulse action of a high power density laser beam on the material in short time intervals, usually in nanoseconds. For thin coatings, laser ablation can be used for removing a part of the coating material (even in the atomic scale) and for reinforcing the remaining part of the coating due to shock wave phenomenon. Very high heating and cooling rates cause grain refinement and the formation of amorphous and nanocrystalline structures. Laser ablation can be used to improve service properties of thin coatings, i.e. to reduce roughness, heal pores and microcracks, increase resistance to wear and microhardness, etc.

2.3. PRODUCTION OF ESD ELECTRODES BY THE POWDER METALLURGY HOT PRESSING ROUTE

The electrodes used to deposit coatings by means of the electro-spark deposition (ESD) method are produced using the powder metallurgy (PM) hot pressing route [22].

2.3.1. Powder mixing and granulating

Basically, the electrode preparation consists in mixing the selected component powders so as to achieve the pre-determined chemical composition, and particle shape and size distribution considering the final product application. This operation is often carried out using chaotic motion mixers (Fig. 2.2).

Binding agents and/or lubricants, e.g. paraffin oil, monoethylene glycol, etc., may often added to the powder at this stage, so as to reduce dust and prevent segregation when the powder is subsequently handled or processed; but also to minimise wear of steel dies and to reduce oxides during subsequent cold and hot pressing operations, respectively.

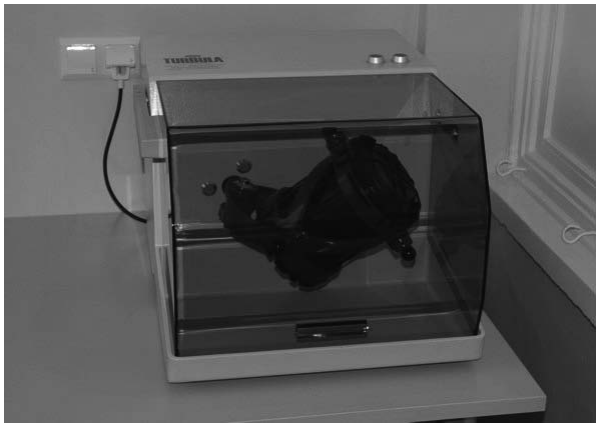

Fig. 2.2. *2 litre Turbula T2C mixer*

When the powder is to be cold compacted on a press working on a volumetric die filling principle, a further granulation treatment is necessary to obtain required flow and packing characteristics of the powder (Fig. 2.3). Granulation may be carried out in a variety of ways [38–42] but, practically, the fluidised-bed method and techniques based on mixing, sieving and rolling have become widespread.

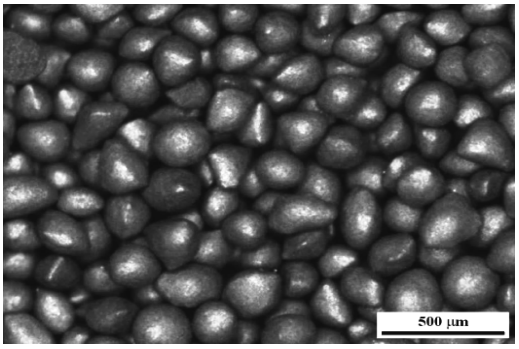

Fig. 2.3. *Fine powder in as-granulated condition*

Irrespective of the processing route, organic binders, e.g. poly (butyl methacrylate), poly (alkyl methacrylate), polyvinyl butyral, paraffin wax, etc., dissolved in suitable solvents, are used to cement the powder particles together, thereby imparting desired mechanical strength to the granules. It is important that the binder has suitable thermal properties, which permit its complete removal from the material at the hot consolidation step.

2.3.2. Cold pressing

Prior to hot pressing, cold pressing may optionally be applied in situations where either the electrode has a layered structure or to increase productivity of the

hot pressing process since, as exemplified in Figure 2.4, the purpose-designed graphite mould yields more sintered parts per hot pressing cycle than the conventional one filled with loose powder.

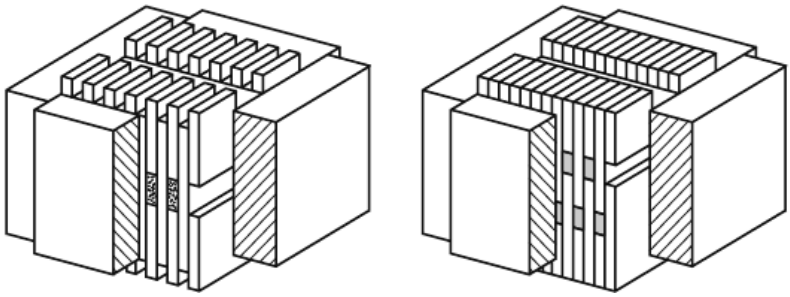

Fig. 2.4. *Graphite moulds designed to accommodate either loose powder mixture (left) or green segments (right)[22]*

Typical cold pressing operations are performed in steel dies, at low to medium pressures, utilising the double-action pressing principle. There are two types of machinery used in the powder metallurgy industry. The conventional presses are fitted with either vibratory or screw powder feeders and precision scales used to weigh out the correct amount of the powder mix to fill the die. Alternatively, the machines may incorporate feed shoes operating on the volumetric filling principle. The gravimetric presses offer higher flexibility necessary to manufacture sintered parts in smaller quantities [43] but, despite higher investment costs attributed in part to obligatory use of granulated powders, the volumetric equipment is the preferred option for mass production due to its 3–4 times greater throughput, longer life of steel dies and lower cost of other pressing consumables [44, 45].

2.3.3. Hot pressing

The hot pressing process consists of a simultaneous application of heat and pressure in order to obtain a product nearly free from internal porosity. Compared to the conventional cold pressing/sintering PM route, hot pressing requires merely 2–3 min hold at markedly lower temperature, but under a compressive stress, to reach higher density level.

The hot pressing of powders, or green compacts, is generally realised in high-resistance graphite moulds by passing electrical current directly through the mould, as schematically shown in Figure 2.5.

This method offers high efficiency in production of sintered parts, at elevated temperatures, assists in protecting metallic powders against oxidation. The protection is attributed to the formation of a CO/CO_2 reducing atmosphere inside the graphite mould which, in the old-type equipment shown in Figure 2.6, is exposed to air.

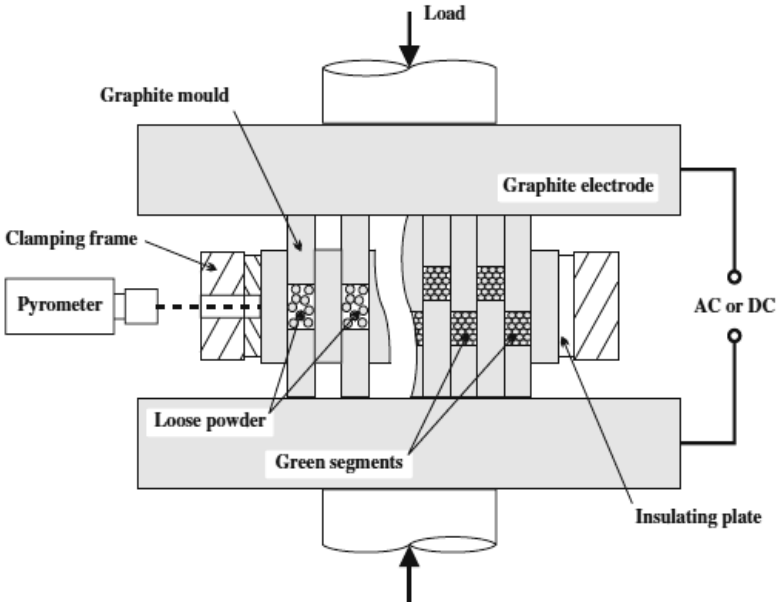

Fig. 2.5. *Schematic representation of the hot pressing process [22]*

Fig. 2.6. *Hot pressing operation carried out in air [22]*

The modern hot presses, exemplified in Figure 2.7, are fitted with protective gas chambers wherein the moulds are heated in nitrogen and therefore their service life is markedly increased.

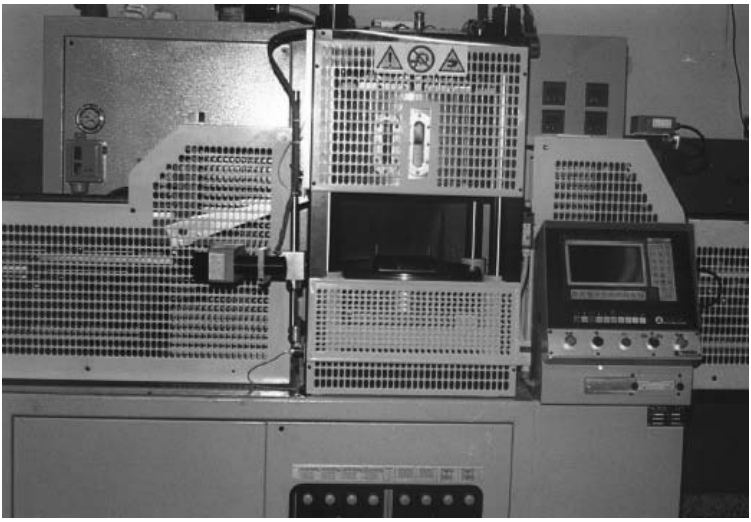

Fig. 2.7. *Hot press equipped with a protective atmosphere chamber [22]*

2.3.4. Deburring, quality control and finishing operations

The vast majority of sintered components require cleaning and removing edge residuals after consolidation. This is carried out during the deburring operation, which is usually performed by means of tumbling the parts extracted from the graphite mould with coarse alumina or silicon carbide grit.

The quality control of sintered electrodes may be limited their visual inspection although, hardness test and evaluation of the as-sintered density may optionally be carried out.

Grinding is usually the final operation which allows attachment of the electrode into a suitable electrode holder of the ESD apparatus.

2.4. MATERIALS AND TREATMENT PARAMETERS

In the experiment, the coatings were electro-spark deposited using a WC-Cu (50% WC and 50% Cu) electrode with a cross-section of 4 mm x 6 mm – the anode – onto samples made of a plain carbon steel C45 – the cathode. The main characteristics of the powders used in this work are included in Table 2.1.

Table 2.1. *Powders used to manufacture WC-Cu electrodes*

Powder	Particle Size, µm	Producer
WC	~0.2*	OMG
Cu	~0.04*	NEOMAT

** measured using Fisher Sub-Sieve Sizer*

The equipment used for electro-spark deposited was an EIL-8A model. Basing on the results of previous research as well as instructions given by the producer, the following parameters were assumed to be optimal for ESA:

- voltage, $U = 230$ V
- capacitor volume, $C = 150$ μF
- current intensity, $I = 0.7$ A.

Then, the coatings were treated with an Nd:YAG laser (impulse mode), model BLS 720. The samples with electro-spark deposited coatings were laser-modified using the following parameters:

- spot diameter, $d = 0.7$ mm
- power, $P = 60$ W
- laser beam velocity, $v = 250$ mm/min
- nozzle-workpiece distance, $\Delta f = 6$ mm
- pulse duration, $t_i = 0.4$ ms
- pulse repetition frequency, $f = 50$ Hz
- beam shift jump, $S = 0.4$ mm
- nitrogen gas shield, $Q = 25$ l/min.

2.5. RESULTS OF INVESTIGATIONS AND DISCUSSION

2.5.1. Measurements of the surface geometric structure and roughness

Surface geometric structure (SGS) substantially influences many processes that occur in the outer layer. A lot of publications deal with measurement methods and the assessment of surface roughness and waviness [46, 47].

Measurements of surface geometric structure were carried out at the Laboratory of Computer Measurements of Geometric Quantities of the Kielce University of Technology. Those were performed using Talysurf CCI optical profiler that employs a coherence correlation algorithm patented by Taylor Hobson company. The algorithm makes it possible to take measurements with the resolution in the axis z below 0.8 nm. The result of measurements is recorded in 1024 x 1024 measurement point matrix, which for the x10 lens yields the 1.65 mm x 1.65 mm measured area and the horizontal resolution 1.65 μm x 1.65 μm.

Three-dimensional surfaces and their analysis with TalyMap Platinum software made it possible to precisely identify the geometric structure of the surfaces under consideration. Table 2.2 provides major parameters of the surface geometric structure of the examined specimens.

Figures 2.8–2.11 present images of surface topography, distribution of ordinates with bearing curves, isotropy diagrams and the specimen autocorrelation function before and after laser treatment.

Table 2.2. *Parameters of the surface geometric structure*

SGS parameters	Coating	
	WC-Cu	**WC-Cu + laser**
Sa, μm	4.02	6.95
Sq, μm	5.24	8.48
Ssk	0.15	0.02
Sku	3.89	2.77
Sp, μm	26.44	34.03
Sv, μm	21.21	66.76
Sz, μm	47.65	100.80

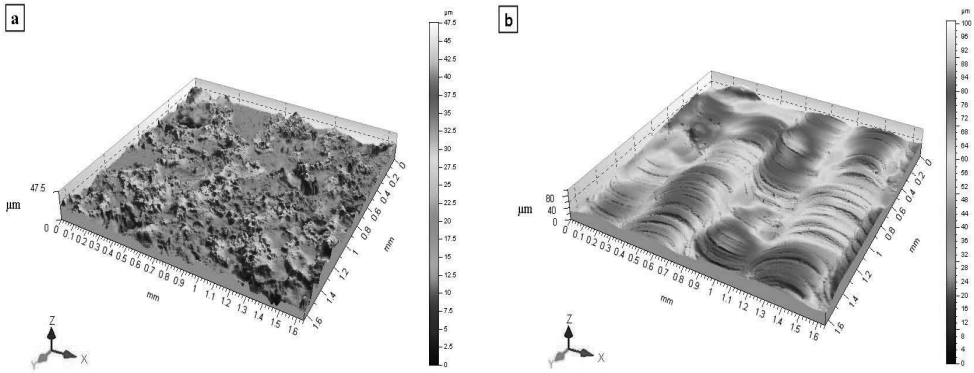

Fig. 2.8. *Specimen surface topography: a) before laser treatment, b) after laser treatment*

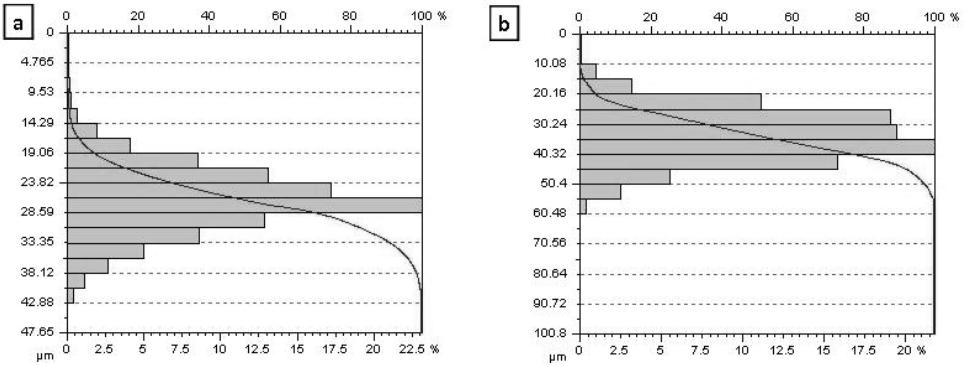

Fig. 2.9. *Distribution of ordinates and specimen bearing curves: a) before laser treatment, b) after laser treatment*

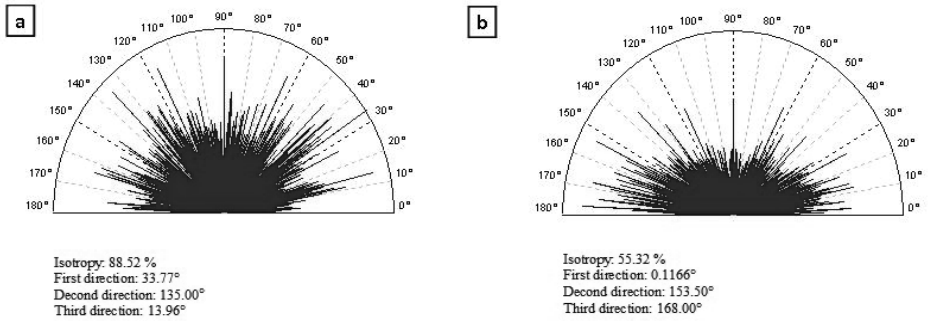

Fig. 2.10. *Specimen isotropy: a) before laser treatment, b) after laser treatment*

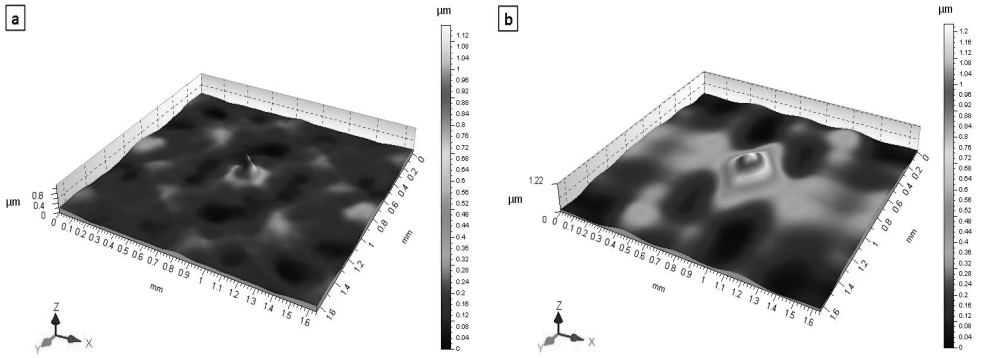

Fig. 2.11. *Specimen autocorrelation function: a) before laser treatment, b) after laser treatment*

A greater value of the mean arithmetic deviation of surface roughness *Sa*, a basic amplitude parameter in the quantitative assessment of the state of the surface under analysis, was recorded for the specimen after the laser treatment, for the specimen before the laser treatment the value of this parameter was be almost 50% smaller.

A similar tendency is observed for the root mean square deviation of surface roughness *Sq*. Complementary information on how the surface of examined elements is shaped is provided by amplitude parameters, namely the coefficient of skewness (asymmetry) *Sku* and the coefficient of concentration (kurtosis) *Ssk*. Those parameters are sensitive to occurrence of local hills or valleys, and also defects on the surface. The parameter *Ssk* has a positive value for both specimens, the value is close to zero for the specimen before treatment, which indicates the symmetrical location of the distribution of ordinates with respect to the mean plane. The values of kurtosis that were obtained are close to *Sku* = 3, which indicates that the distribution of ordinates for both specimens is close to normal distribution.

Before laser treatment, the specimen had random isotropic structure (Iz = 88.52%), whereas after the treatment, that became a periodic structure, located in the transient area between isotropic and anisotropic structures (Iz = 55.32%). That is confirmed by the shape of the autocorrelation function of both surfaces, for the

surface before treatment, the shape is circular and symmetrical, whereas for the surface after treatment, it is asymmetrical and elongated.

The roughness of the WC-Cu coatings was quantitatively assessed using the Talysurf CCI optical profiler. Roughness profiles are routinely measured by dragging a stylus along the laser beam path whereas the maximum values of the arithmetic average departure from the surface plain are reported to occur in the perpendicular direction. Therefore in this study an average value of Ra was calculated for each coating from readings taken on evenly divided sampling lengths running parallel to the electrode/laser beam motion and on similar lengths at 90º. It was found that the employed surface treatments increased the average roughness value (Ra) from 0.41–0.44 μm for the C45 steel substrate up to 2.37–3.67 μm and 3.05–4.26 μm for the WC-Cu coatings in as-deposited and laser treated condition, respectively.

Figures 2.12 and 2.13 presents an example two-dimensional surface microgeometry measurement of the WC-Cu coatings before and after laser treatment.

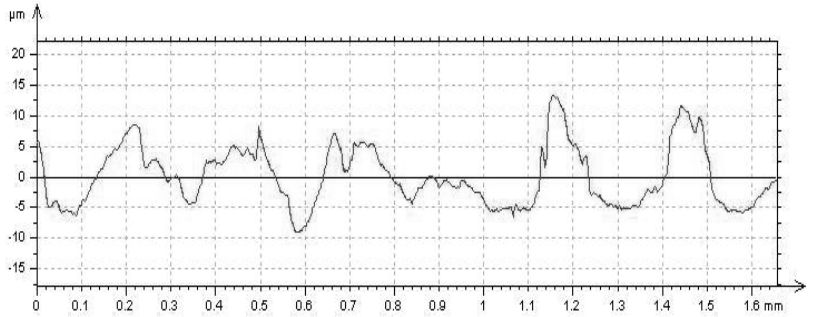

Fig. 2.12. *Surface microgeometry of the WC-Cu coating deposited*

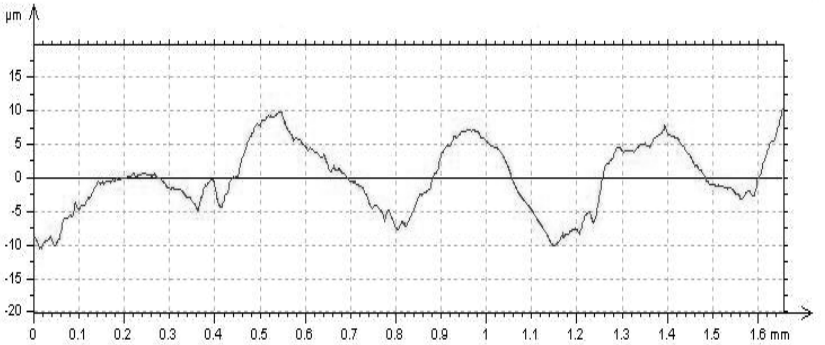

Fig. 2.13. *Surface microgeometry of the WC-Cu coating deposited after laser treatment*

It is evident from the measurements that there is an increase in roughness of the WC-Cu coatings after laser treatment. The higher roughness resulted from the tensile forces acting on the surface, and accordingly, the motion of the liquid metal. A non-uniform distribution of temperature in a laser beam (mod TEM_{00}) caused the

non-uniformity of the surface profile after solidification, which, to some extent, reflects the distribution of energy in the melted zone. If pulse laser treatment is applied, it is assumed that the main factor affecting the surface profile after solidification is the pressure of vapor causing the disposal of the material from the central zone and the production of characteristic flashes on the boundary between the melted and unmelted zones.

2.5.2. Tribological tests

Investigations into dry friction resistances were performed using the T-01M pin-on-disk type tribotester. The specimens were rings of C45 carbon special steel, onto which WC-Cu coatings (before and after laser treatment) were electro-spark deposited. The counter specimen was a ball, ∅6.3 mm in diameter, made of 100Cr6 steel.

Tribological tests were conducted using the following parameters:

- linear speed, $v = 0.8$ m/s
- test duration, $t = 3600$ s
- range of load changes, $Q = 4.9$; 9.8; 14.7 N.

An exemplary graph (Fig. 2.14) shows friction coefficient profiles as a function of time for the load of 14.7 N. The graph presented in Figure 2.14 refers to the tests on WC-Cu coating before and after modification with a laser beam.

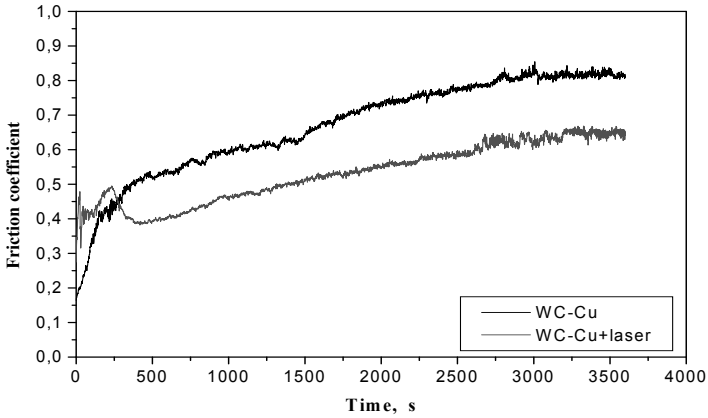

Fig. 2.14. *Friction coefficient as a function of time*

In dry friction, in the examined coating, the technological surface layer (TSL) was transformed into a functional surface layer (FSL). The effect was produced mainly due to sliding stresses and speed and the action of the atmosphere of the environment close to the tested surface. The stabilisation of the state of anti-wear surface layer was observed (AWSL).

In the profile (Fig. 2.14) that refers to the WC-Cu coating, it can be seen that the stabilisation of the friction coefficient takes place after approx. 3.000 seconds, the

stabilisation value ranges between 0.80–0.82. As regards the WC-Cu coating after laser modification, one can see that the stabilisation of the friction coefficient occurs after 3200 seconds, and the friction coefficient stabilises at 0.61–0.64. The average friction coefficient of the WC-Cu coating is approx. 22% higher than the friction coefficient of the WC-Cu coating after laser irradiation. This effect might be produced due to the elimination of surface defects (microcracks and pores) by the laser treatment.

Seizure resistance tests were carried out using T-09 tribotester, in which the friction pair consisted of a cylinder and two prisms. Prisms with deposited WC-Cu coatings and C45 steel (laser treated and untreated) acted as specimens, whereas a roller of hardened carbon steel, ∅6.3 mm in diameter, was used as a counter-specimen. In tests, three kinematic pairs were employed to investigate different material options, which made it possible to average experimental results. During the test, paraffin oil bath lubrication was used.

Figure 2.15 presents cumulative information on average values of seizure load for specimens before and after laser treatment. Those indicate that laser treatment resulted in an increase in the load that produced seizure both for electro-spark deposited coatings and for C45 steel.

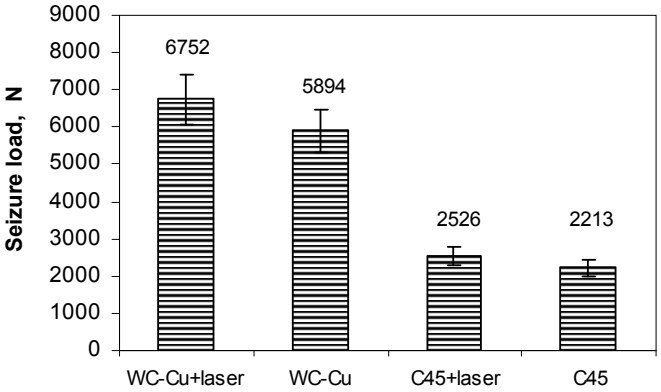

Fig. 2.15. *Average values of seizure load*

Exemplary graphs (Fig. 2.16) show the dependence of load and friction values as a function of time as recorded in the tests. The patterns are typical of seizure tests conducted with T-09 instrument. An increase in the load is accompanied by a respective increase in friction force. Consequently, increasing the load applied to the sliding pair leads to such an increase in the friction force that the copper pin is broken and the test is interrupted. The maximum value of the load, at which seizure occurs and the time that elapsed from the beginning of the test, can be read from the graphs recorded.

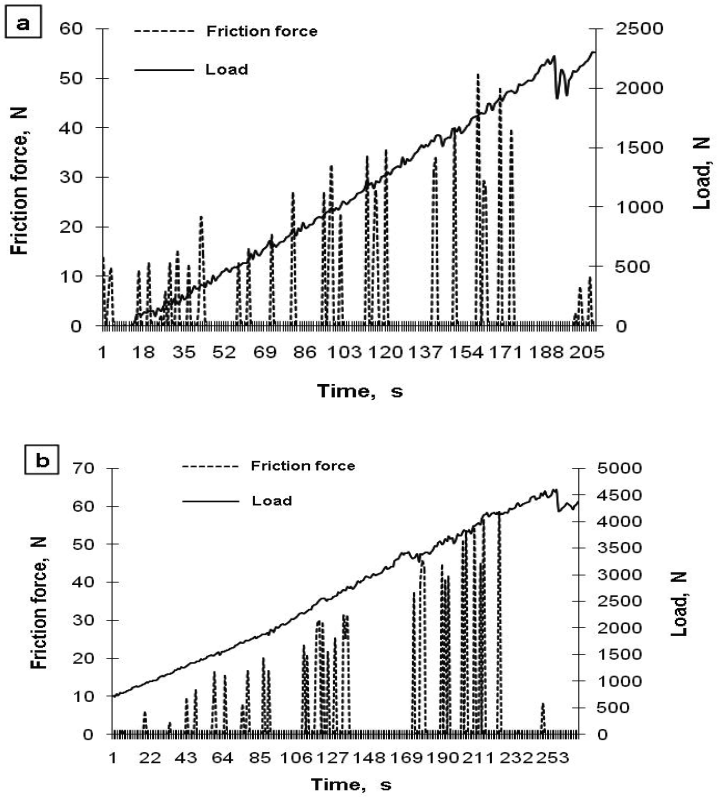

Fig. 2.16. *Dependence of friction force and load as a function of time: a) C45 steel, b) WC-Cu coating*

2.5.3. Analysis of the coating microstructure

A microstructure analysis was conducted for WC-Cu coatings before and after laser treatment using a scanning electron microscope Joel JSM-5400.

Figure 2.17 shows the microstructure of an ESD WC-Cu coating. It is clear that the thickness of the obtained layer varied from 36 to 60 μm, whereas the heat affected zone (HAZ) ranged from 20 to 30 μm into the substrate. Figure 2.17 also reveals a clear boundary between the coating and the substrate and pores within the coating. The ESD WC-Cu coatings were modified by the laser treatment, which caused changes in their composition. The laser treatment homogenizes the coating chemical composition, causes structure refinement, and crystallization of non-equilibrium phases due to the occurrence of temperature gradients and high cooling rates.

The laser-modified outer layer does not possess microcracks or pores (Fig. 2.18). There is no discontinuity of the coating-substrate boundary. The thickness of the laser-treated WC-Cu coatings ranges from 40 to 62 μm. Moreover, the heat affected zone (HAZ) is in the range of 25 to 35 μm, and the content of carbon in the zone is higher.

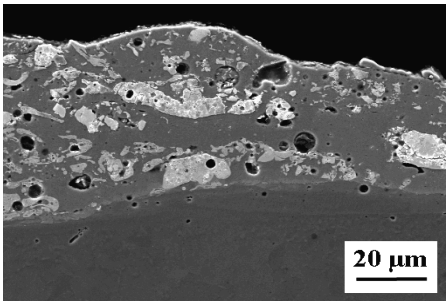

Fig. 2.17. WC-Cu coating microstructure after electro-spark alloying

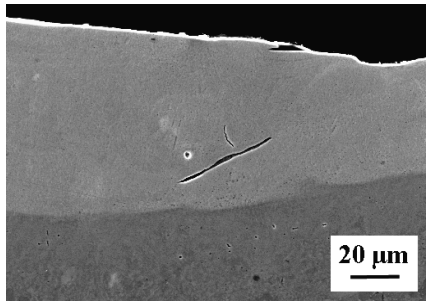

Fig. 2.18. Microstructure of the electro-spark alloying WC-Cu coating after treatment with an Nd:YAG laser

2.5.4. X-ray diffraction analysis

Using the X-ray diffraction method, the analysis of the phase composition of the examined coatings was performed with Philips PW 1830 instrument. Cu Kα filtered radiation was employed. Tests were carried out for the 2θ angle in the range 30–60° and the scanning velocity of 0.05°/3 seconds.

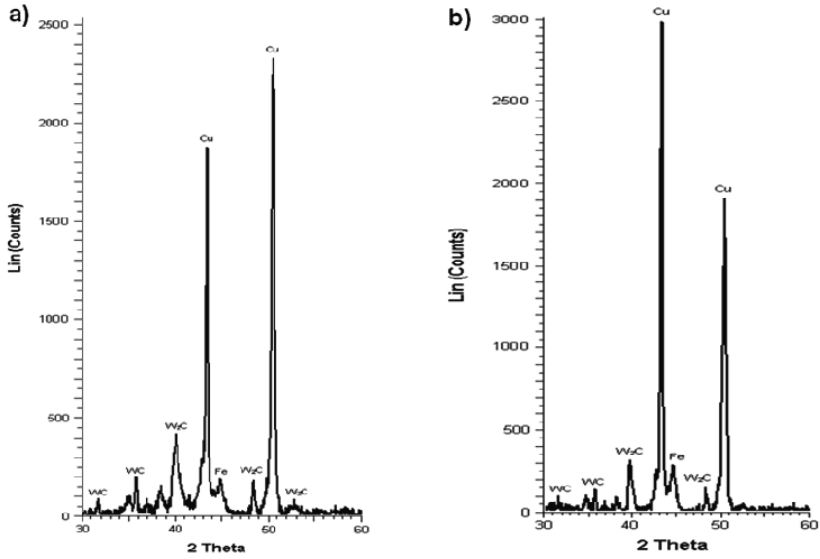

Fig. 2.19. X-ray diffraction pattern of the WC-Cu coating: a) before laser treatment, b) after laser treatment

The analysis of the phase composition of the WC-Cu coating (Fig. 2.19a) revealed that the surface layer of the coating consisted mainly of Cu and W_2C and a small amount of WC and Fe. Laser treatment did not cause the melting of the WC-Cu coating to penetrate into the substrate material (Fig. 2.19b). The surface

layer of the WC-Cu coating after laser treatment has the same composition as that of the coating before the treatment. The most intense peaks originate from Cu (Fig. 2.19a and 2.19b).

2.5.5. Microhardness tests

The microhardness was determined using the Vickers method (Microtech MX3 tester). The measurements were performed under a load of 0.4 N. The indentations were made in perpendicular microsections in three zones: the white homogeneous difficult-to-etch coating, the heat affected zone (HAZ) and the substrate. The test results for the electro-spark deposited WC-Cu coating before and after laser treatment are shown in Tables 2.3 and 2.4. Electro-spark deposition caused changes in the microhardness of the material. The microhardness of the substrate after electro-spark deposition was 278 HV0.4; the same value was reported for the substrate before the process. There was a considerable increase in microhardness after depositing the WC-Cu coating. The microhardness of the WC-Cu coating was approx. 643 HV0.4. The microhardness of the WC-Cu coating in the heat affected zone (HAZ) after electro-spark treatment was 58% higher than that of the substrate material. Laser treatment had a favorable effect on the changes in the microhardness of the electro-spark deposited of the WC-Cu coating. There was an increase of 122% in the microhardness of the WC-Cu coating.

Table 2.3. *Results of the microhardness tests for the WC-Cu coating before laser treatment*

Measured zones	Microhardness HV0.4			Mean value* HV0.4
	Measurement number			
	1	2	3	
Coating	652	691	585	643 ±54
HAZ	428	464	421	438 ±23
Substrate	262	297	275	278 ±18

*scatter intervals estimated at 90% confidence level

Table 2.4. *Results of the microhardness tests for the WC-Cu coating after laser treatment*

Measured zones	Microhardness HV0.4			Mean value* HV0.4
	Measurement number			
	1	2	3	
Coating	594	621	635	617 ±21
HAZ	391	397	432	407 ±22
Substrate	276	288	273	279 ±8

*scatter intervals estimated at 90% confidence level

Conclusions:

1. A concentrated laser beam can be effective in modifying the state of the outer layer of electro-spark coatings and thus can modify their functional properties.
2. Laser irradiation of coatings resulted in the healing of micro-cracks and pores.
3. Parameters of surface geometric structure of electro-spark coatings have lower values when compared with SGS parameters of coatings after laser treatment.
4. The surface layer of the WC-Cu coating before and after laser treatment consists mainly of Cu and W_2C and a small amount of WC and Fe.
5. The average friction coefficient obtained for WC-Cu coating in tribological tests is approx. 22% higher than the friction coefficient of the WC-Cu coating after laser modification.
6. Laser treatment caused an increase in the load at which seizure occurred for the tested materials. For laser-treated WC-Cu coatings, the value of the load is approx. 13% higher when compared to coated specimens without laser treatment.
7. Laser treatment caused a 9% decrease in the microhardness of the electro-spark alloying WC-Cu coatings.

Coatings of that type can be applied to sliding friction pairs and can operate as protective coatings.

Further research should involve measurements of internal stresses and investigations into the porosity of electro-spark coatings before and after laser treatment.

3. PRODUCTION OF HETEROGENEOUS SURFACES BY ELECTRO-SPARK DEPOSITION AND LASER BEAM MACHINING

3.1. HETEROGENEOUS SURFACES

During tribological investigations it was found that employing heterogeneous surfaces models into boundary interaction of solid surfaces could make significant improvement [48]. Surfaces described as heterogeneous consist of areas, which are different one from another in geometrical, physicomechanical or physicochemical properties. The heterogeneity of surfaces is frequently due to the application of more than one technology, and can be constituted by [49–58]:

- shaped surface features such as grooves, pits or channels resulting from milling, eroding, etching, laser-beam forming, etc.,
- areas with different physicochemical and physicomechanical properties, e.g. areas with varying hardness and mechanical strength accomplished by local surfacing or selective surface hardening (e.g. electron-beam machining, laser-beam forming or thermochemical treatment),
- areas with diversified surface microgeometry, e.g. areas eroded at the points of focus (laser treatment or electro-spark deposition), or areas with formed surface microgeometry, for instance, in terms of desired microroughness directivity or load capacity (LBM and ESD technologies).

Heterogeneous surfaces can be obtained by different methods. The laser treatment of electro-spark deposited coatings being one of them [54, 56].

The first publication on surface texturing appeared in Germany in 1993 [59]. It discussed the use of an excimer laser to texture elements of a magnetic memory disk drive with the aim of reducing friction at the start. Further experiments in this area involved texturing surfaces of punches applied to plastic forming. It was found that the process caused a 169% increase in the punch service life.

The current studies focus on the influence of texturing on the performance of various friction systems in internal combustion engines, e.g. precision bearing systems. Texturing is used to improve heat removal, vaporization, wettability, biological functions, absorptivity, etc.

Reference [60] analyzes the relationships between the parameters of performance and the parameters of surface texture for a mechanical seal. In this model approach, the considerations involve solving the Reynolds equation transformed into a dimensionless form for a face seal with one textured ring. The texture is created by a number of circular pores. The radius of a pore is several times greater than the depth. The results of the theoretical investigations are presented in the form of dimensionless relations, including the ratio of the cavity depth to the cavity diameter and the ratio of the area with pores to the whole surface area (pore area coverage) as well as the dimensionless pressure and the leak tightness, Λ.

$$\Lambda = \frac{6 \cdot \mu \cdot U \cdot r_p}{p_a \cdot C^2} \tag{3.1}$$

where: μ – fluid dynamic viscosity, Pa · s; U – sliding velocity, m/s; p_a – ambient pressure, Pa; C – clearance height, m; r_p – cavity diameter [m].

The references quoted in this paper indicate that the cavity diameter and the pore area coverage have a negligible effect on the average pressure in the clearance. Of importance, however, seems to be the depth-to-diameter ratio, which can be optimized for the pre-determined parameter Λ. From the analysis it is clear that the effectiveness of micropores depends on the relationships between the hydrostatic and hydrodynamic effects. If the cavitation in micropores is eliminated by applying suitable parameters of performance, then the hydrostatic effects predominate and the effect of laser texturing is not significant; in consequence**,** the surfaces behave like non-textured ones.

An increase in the parameter Λ causes that the hydrodynamic effect of microcavities is more visible. The effect is determined basing on the value of the average pressure in the clearance. In addition, there is an optimal value of $h_p/2r_p$, which is equal to 0.05 for $\Lambda = 1$, and decreases with an increase in the parameter Λ.

Reference [61] compares results of tribological tests conducted by means of pin-on-disk testers, where the disk surfaces were polished, ground and textured using three methods of texturing. The textured surface was covered with laser-generated pores, 4–6.5 μm in depth and 58–80 μm in diameter. Numerous tests show that texturing can be used to extend the range of load and sliding velocity wherein hydrodynamic lubrication occurs. The hydrodynamic lubrication is observed when low- and high-viscosity lubricants are applied. Another finding is that the rough rims of cavities produced by laser beams need to be removed by lapping to ensure an optimal hydrodynamic effect. A comparative analysis was conducted to determine the friction coefficients for the polished, ground and textured surfaces. The effects of laser texturing were most visible when the values of sliding velocity were low, ranging between 0.075 and 0.3 m/s. Moreover, the high density of cavities was responsible for an increase in the friction coefficient. The results presented in the form of Stribeck curves illustrate that there was a significant reduction in friction for lubricated friction pairs operating in the boundary regime of friction.

The tests described in ref [62] aimed at determining the effect of laser texturing on the performance of a ring being in contact with a cylinder liner. Pores with diameters of 75–78 μm and depths of 7–9 μm covered the whole or part of the ring surface. The pore area coverage ranged between 10 and 50%. The friction observed for textured surfaces was lower than that for non-textured ones. The greatest falls in friction were reported for a pore area coverage of 30%; they were 40–45% and 23–35% for a rotational speed of 500 rev/min and 1200 rev/min, respectively. It should be noted that the decrease in friction was greater for a partly textured ring. This reduction (12–29%) was observed in the whole range of loads and rotational speeds.

Reference [63] discusses results of in-service tests conducted for face seals with textured carbide rings used in the petrochemical industry. The results were positive, because there was a decrease in the process temperature and an increase in the ring service life. Reference [64] illustrates that laser surface texturing caused an improvement in fretting fatigue life of steel tool elements.

This analysis shows that the effects of laser texturing were measured at predetermined parameters of performance of the sliding pair; the pore depth and diameter (or their ratio) and the pore area coverage were the most significant parameters of texturing. It was found that effective reduction in friction could be obtained also for partially porous surfaces. The problems to be solved in further research include determining precisely the relationships between the texturing parameters, ring geometry, and the parameters of performance of the friction system for which the desired reduction in friction occurs. The current research focuses on establishing the effect of laser surface texturing on the mechanical properties of materials, particularly their fatigue strength.

3.2. EXPERIMENTAL

A two-stage investigation was carried out. First, Cu-Mo coatings were electro-spark deposited on C45 steel coupons and after that they were modified by Nd:YAG laser beam. The copper inside coatings is being fundamental material to created of low-friction surface layers. It is itself also internal stresses compensator. This material is characterized by good thermal conductivity, which can be very helpful in high loaded contacts – heat can be taken away into the material core from the friction zone. The other element, molybdenum, was used to strengthen the surface. Mo is also helpful in creation of hard phase compounds, e.g. MoC. In practical meanings this compound will improve durability of tool kinematics pairs. The electro-spark deposition of Cu and Mo wires with a diameter of 1 mm was performed by means of an ELFA-541, a modernized device made by a Bulgarian manufacturer.

The subsequent laser treatment was performed with the aid of a BLS 720 laser system employing the Nd:YAG type laser operating in the pulse mode.

The parameters of the electro-spark deposition established during the experiment include:

- current intensity, $I = 16$ A (for Cu $I = 8$A)
- table shift rate, $v = 0.5$ mm/s
- rotational speed of the head with electrode, $n = 4200$ rev/min
- number of coating passes, $L = 2$ (for Cu $L = 1$)
- capacity of the condenser system, $C = 0.47$ μF
- pulse duration, $t_i = 8$ μs
- interpulse period, $t_p = 32$ μs
- frequency, $f = 25$ kHz.

The main objectives of the investigations were:
- observing the surface state by means of a stereoscopic microscope
- microstructure analysis by means of a scanning electron microscope
- analyzing the surface macrogeometry
- measuring the microhardness with the Vickers method.

3.3. RESULTS AND DISCUSSION

The heterogeneous Cu-Mo coatings structure after electro-spark deposition on steel coupons and eroded by laser beam were investigated. The observation was done by OLYMPUS SZ-STU2 stereoscopic microscope.

The erosion was performed with the point pulsed-laser technique using the Nd:YAG type laser under the following conditions:
- laser spot diameter, d = 0.7 mm
- laser power, P = 10; 20; 30; 40; 50; 100 and 150 W
- beam shift rate, v = 1200 mm/min
- nozzle-sample distance, h = 1 mm
- pulse duration, t_i = 0.8; 1.2; 1.48; 1.8; 5.5 and 8 ms
- frequency, f = 8 Hz.

As can be seen from Figures 3.1 and 3.2, the effect of the laser erosion action is in the form of craters. The first one is showing lower laser power (P = 20 W) interaction effect on the treated surface (Fig. 3.1). The second one is illustrating phenomenon (Fig. 3.2), where the laser power was increased 5 times (P = 100 W). The cavity depth depends mainly on the laser power density and the pulse duration. Coatings with such geometry have various tribological applications. By rubbing the surface selectively, it is possible to produce cavities inside which hydrodynamic forces can be generated during fluid film lubrication. Moreover, the hard areas around the cavities are capable of bearing normal loads.

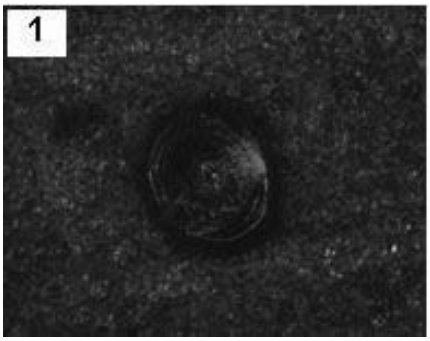

Fig. 3.1. *Stereoscopic photograph of a Cu-Mo coating laser-eroded at 100 W (x57 magnification)*

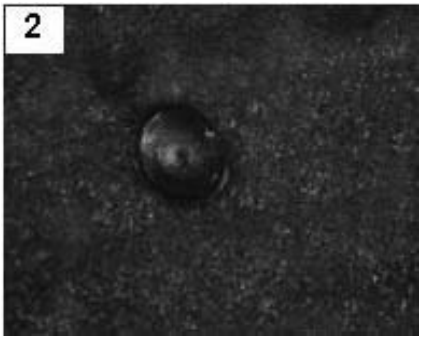

Fig. 3.2. *Stereoscopic photograph of a Cu-Mo coating laser-eroded at 20 W (x57 magnification)*

The investigations of the effects of the laser erosion involved measuring the diameters and depths of the cavities obtained at different laser powers. The results of the measurement performed with a PG-2/200 form surfer are presented in the form of graphs in Figures 3.3 and 3.4. It was noticed that higher laser beam power gives greater diameter and depth of the cavities. An exception is the cavity depth produced at 150 W. The value is smaller than that obtained at 100 W (Fig. 3.3). This might have been due to a considerable pulse duration (t_i = 8 ms), the laser power being 150 W. However, if P = 100 W, the pulse duration t_i was 5.5 ms. In the case of lasers operating in the pulse mode, the power is averaged in time; thus, if the pulse durations are long, the laser beam is less effective.

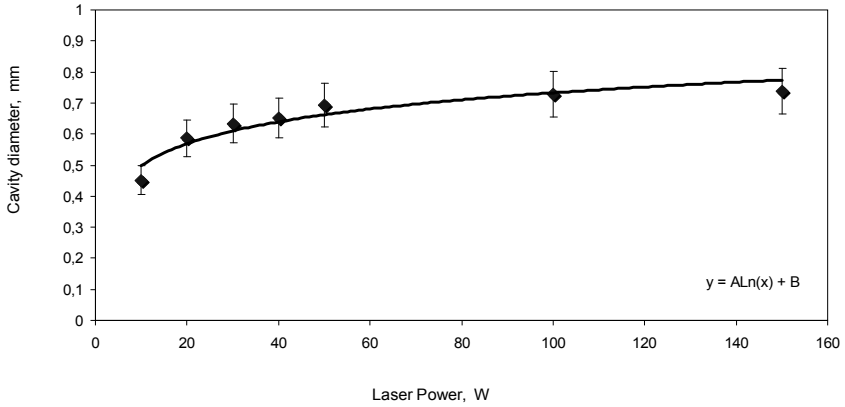

Fig. 3.3. *Cavity diameter as a function of laser power*

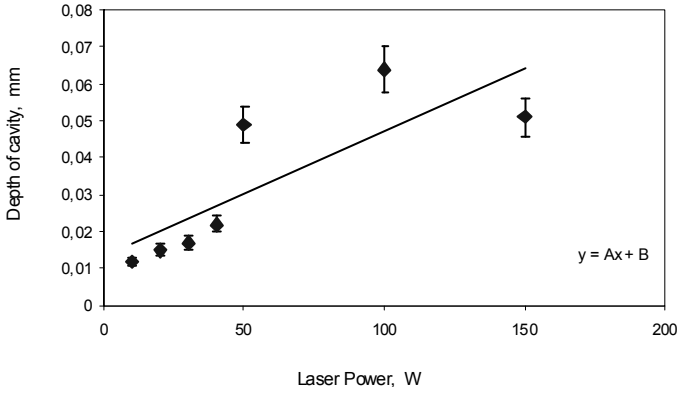

Fig. 3.4. *Cavity depth as a function of laser power*

A 3D macrogeometry of the developed heterogeneous surface eroded by the laser craters for the used specimens with build in 2-D crater cross section A-A (Fig. 3.1) is shown in Figures 3.5a and 3.5b. As can be concluded from these graphs, crater edges are sharp and are protruding 0.03 mm above an average height, just treated by ESD surface, what is within a range of tolerances for designed

clearance fit. The average size of the crater shown on Figure 3.1 produced by laser power 100 W is about 0.7 mm in diameter and the total depth about 0.06 mm. The crater is going below so-called "ground zero level" by down to 0.030 mm. For instance, crater displayed in Figure 3.2, produced by laser power 20 W, is about 0.05 mm in diameter and has a depth of 0.015 mm. Produced crater profile (picks and valleys) and also order of craters location, depending on the required or desired surface performance, could be controlled and adjusted to acceptable level.

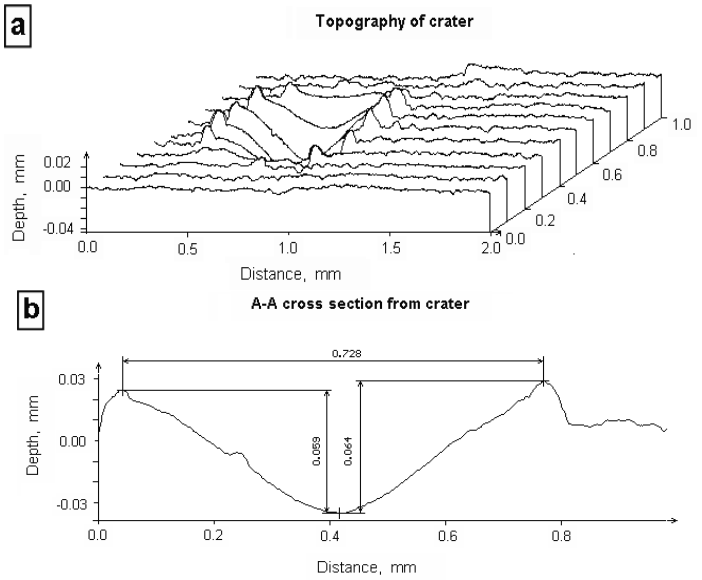

Fig. 3.5. *Macrogeometry and cross section of a crater eroded by laser: a) 3D crater topography; b) A-A cross section on Figure 3.1*

At the next stage, the Vickers microhardness test was conducted using a load of 0.98 N. The measurements was carried out on Cu-Mo coatings laser-eroded at 20 W. The distribution of microhardness is shown in Figure 3.6.

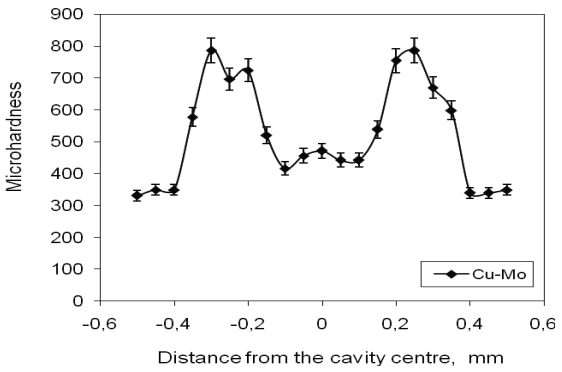

Fig. 3.6. *Distribution of microhardness on the surface of a laser-treated Cu-Mo coating*

It was established that there was an increase in microhardness at the points of laser machining, the increase being strictly related to the changes in the coating structure, and therefore, to the method of laser treatment. The surface hardening at the points of laser interaction and in the heat-affected zone (HAZ) follows the phase changes occurring in the material first heated and then immediately cooled. The average microhardness of the C45 steel substrate was 300 HV. That of the ESD coatings amounted to about 430 HV. The laser treatment of the ESD coatings caused an increase in microhardness to approximately 850–880 HV. In the heat-affected zone, the microhardness fluctuated around 580–630 HV. The laser beam surface forming resulted in changes in the microhardness of electro-spark deposited Cu-Mo coatings.

The next stage of the experiment involved analyzing the changes in the macrogeometry of Cu-Mo coatings. The laser treatment causing the formation of new surface geometry was performed with the BLS 720 Nd:YAG laser operating in the pulse mode, with the process parameters being:

- laser spot diameter, $d = 1.5$ mm
- laser power, $P = 30$ W
- beam shift rate, $v = 250$ mm/min
- nozzle-sample distance, $h = 1$ mm
- pulse duration, $t_i = 0.8$ ms
- frequency, $f = 8$ Hz.

An image obtained with a stereoscopic microscope for laser-treated Cu-Mo coatings is given in Figure 3.7.

Fig. 3.7. *Stereoscopic photographs of the laser-treated Cu-Mo surfaces (x40 magnification)*

The investigations of the microgeometry were conducted by means of the PG-2/200 form surfer. The instrument makes it possible to measure the surface form using a contact method and to obtain a 3-D isometric image and a contour map. The isometric image presents a selected fragment of the surface measured in the form of a series of finite profiles displaced by a certain constant vector. The contour map, on the other hand, consists of lines connecting points, each one lying at the same distance from the reference surface. To measure the macrogeometry of

Cu-Mo surfaces after laser treatment, it was essential to select a plane with an area of 3 mm by 3 mm.

Figures 3.8 and 3.9 show an example profile and isometric image of a Cu-Mo coating after laser treatment. The convexities visible in Figures above are marks of laser beam passes. The regular intervals between paths constitute a specific surface structure. The first one in Figure 3.8 is showing two dimensional surface macrogeometry of a Cu-Mo coating after laser treatment.

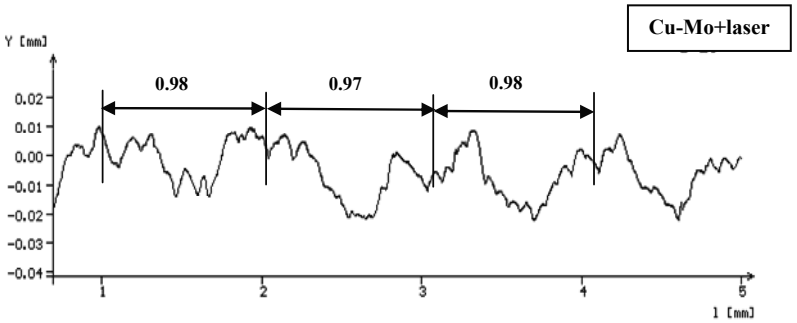

Fig. 3.8. *Two dimensional surface macrogeometry of a Cu-Mo coating after laser treatment*

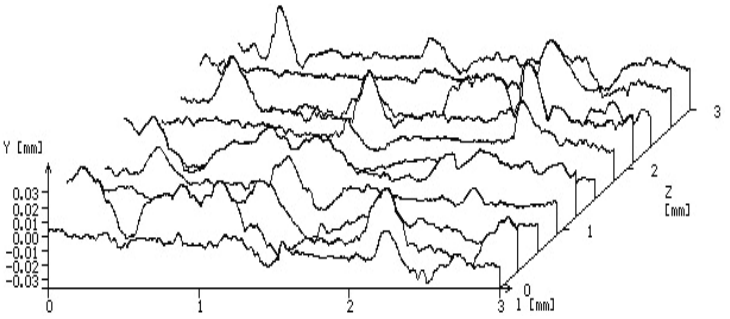

Fig. 3.9. *Three dimensional surface macrogeometry of a Cu-Mo coating after laser treatment*

Figure 3.9 shows that the structure is characterized by the occurrence of enclosed areas of cavities with dimensions of approximately 0.98 mm by 0.98 mm. To be used in tribological applications the coatings require additional treatment, i.e. grinding. As a result the concavities become flat and hard areas able to bear normal loads. The difference in surface levels before and after the operation amounts to 10 μm and is due to changes in the structure and the specific volume in the zones of laser beam heat impact. The second profile in Figure 3.9 is presenting three dimensional surface macrogeometry of a Cu-Mo coating after laser treatment.

A Joel JSM-5400 scanning microscope equipped with an Oxford Instruments ISIS-300 X-ray microanalyzer was used to test the coating microstructure. Figures 3.10a show the microstructure of electro-spark deposited two-layer Cu-Mo coating. The layer thickness is approximately 8–10 μm, and the range of the heat affected zone (HAZ) inside the (underlying) substrate material is about 10–15 μm. In the

photograph, the boundary line between the two-layer coating and the substrate is clear. There are microcracks running across and along the coating. A linear analysis of the elements (Fig. 3.10b) of the Cu-Mo coating shows that the distribution of elements is non-uniform; there are zones with greater concentrations of Cu, Mo and Fe. Analyzing the linear distribution of elements, one can see that the adhesion of the coating to the substrate is of diffusive type. There is no clear separation of components in the Cu-Mo coating (Fig. 3.10b). A higher content of carbon reported in the electro-spark deposited Cu-Mo coating is a result of diffusion. Carbon from the C45 steel substrate travels to the electro-spark deposited technological surface layer (TSL) because of thermal interaction.

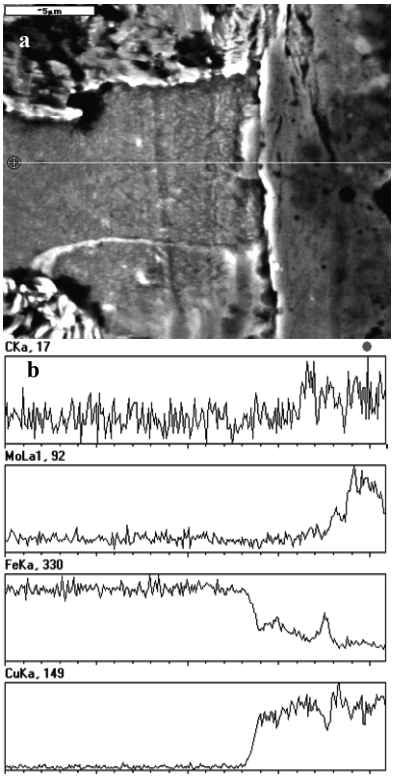

Fig. 3.10. *Microstructure (a) and linear distribution of elements (b) in the Cu-Mo coating*

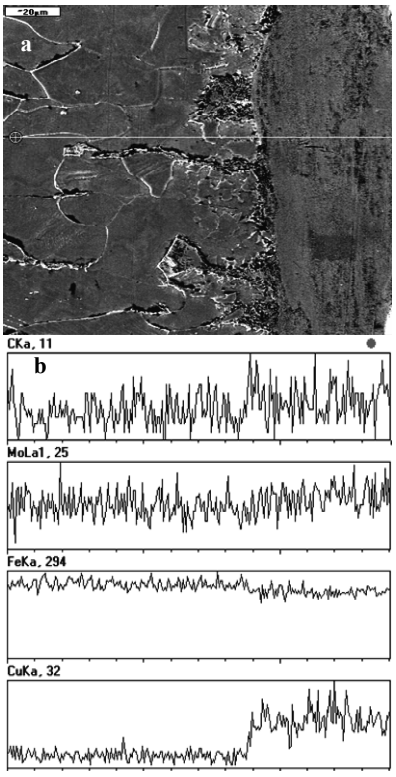

Fig. 3.11. *Microstructure (a) and linear distribution of elements (b) in the Cu-Mo coating after laser treatment*

The melting and solidification processes during laser treatment resulted in the migration of elements across the coating-substrate interface. Laser radiation caused intensive convective flow of the liquid material in the pool and, in consequence, the homogenization of the chemical composition (Fig. 3.11b). It also led to the structure refinement and highly saturated phase crystallization (Fig. 3.11a) because of considerable gradients of temperature and high cooling rates. The technological

surface layers, produced by laser alloying, were free from microcracks and pores – an effect of surface sealing, and non-continuities across the coating-substrate interface. The thickness of the fused two-layer Cu-Mo coating ranged 20–40 μm. In the heat affected zone (HAZ), which was 20–50 μm thick, there was an increase in the content of carbon (Fig. 3.11b).

The point analysis conducted for the outer surface of the technological surface layers (TSLs) (Fig. 3.12a) shows high intensity of peaks of the elements present in the coating. The Cu-Mo coating contained 66.07% at. of Cu and 10.98% at. of Mo, which may testify to the mixing of the two elements and the formation of a multi-phase alloy (Fig. 3.12a).

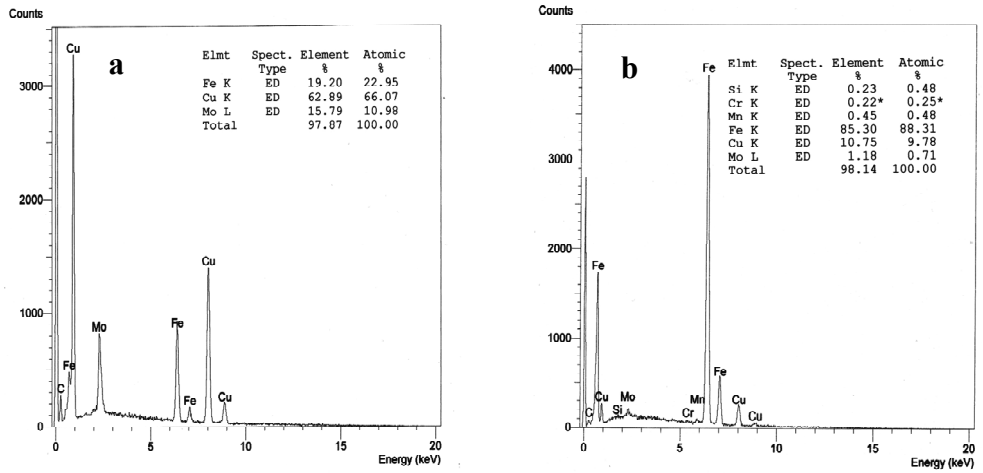

Fig. 3.12. *Spectrum of an X-ray radiation for an electro-spark deposited Cu-Mo coating on a C45 steel substrate: a) before laser treatment, b) after laser treatment*

The point analysis of the electro-spark coatings treated with a laser beam (Fig. 3.12b) shows high intensity of iron peaks in the alloyed layers. The content of iron in the laser-treated technological surface layers was between 88% at. and 97% at. After laser treatment, the intensity of Mo and Cu peaks in the electro-spark deposited coatings was lower.

3.4. MOBILITY OF FRETTING CONTACT AFTER LASER MELTING OF SURFACE

Significant changes in the ideology of modern production and operation of mechanical systems are related to the rapid development of computer technology. Exceptionally important role is given to the structural integrity of the nominally-fixed frictional joints [65]. Nowadays this area is developed on the basis of classical mechanics of solid body (for example, the calculation of interference fits), theory of elasticity [66], solid state physics fields of nonlinear contact dynamics, tribology, theory of chaotic oscillations, stochastic theory describing

microgeometry of surfaces, low amplitude fretting, nanotechnology and so on. The attention is focused on micromotion with microslip [67–69]. It is a logical step in researching of the origin of cracks, plastic deformation and, ultimately, solving the complex problems concerning integrity of nominally-fixed joints and surface modification of important structures and units.

An integral and important part of the problem of integrity of the nominally-fixed frictional joints is a factor of cyclic relative microdisplacements in contact. These phenomena are the subject of special studies of many researchers in mathematics, physics, optics, mechanics, electromechanics. At the beginning of the last century tribological side of these phenomena was presented in a single concept as **fretting of contact surfaces** [70, 71]. Since the middle of the twentieth century fretting was investigated in the direction of increasing longevity and reliability of machine parts.

Fretting is commonly observed on the assembly interfaces of mechanical power transmission components. Typical examples include spline couplings, bearing/housing interfaces and gear/flange interfaces [72]. The fretting action can be caused by shaft misalignments as in the case of spline wear or by mechanical strain differences between mating components, as for gear/flange interfaces. In any event, the occurrence of fretting is marked by the surface damage that may include crack initiation, pitting, and debris generation. The consequences often include degradation of component fatigue life, loss of critical assembly tolerance and fouling of moving components by debris [73]. Both the extent of fretting damage and the mechanisms of fretting are affected by a number of factors including slip amplitude, relative humidity, temperature, fretting frequency, normal load, and the materials comprising the fretting pair.

The method ensures the impact of surface modification and creates a regular relief on the surfaces in long-term ability to maintain the integrity of contact under vibration loads.

Reliability and durability of equipment connect with the need to ensure adequate quality of individual units and elements of their interface as in the case of **nominally-fixed joints (NFJ)**. It is achieved by applying coatings. But usually it changes the properties of the surface layer.

There are many methods applied for modifying surfaces. But it remains unclear what impact the macrogeometry of surface has on the long-term ability to maintain the integrity of contact. Macrogeometrical characteristics are especially important for the initial conditions of the contact as significant affect of the elastic characteristics of contact and, consequently, tribological characteristics of the joints.

Surface profile is formed by high-energy methods such as laser and electric-sparks treatment which have the character of regular micro and macro irregularities.

Therefore, for quantitative and qualitative assessment of the working surface from a position of long-term conservation of the nominal contact of parts of joints. On the design stage, it is expedient to apply the methods of mathematical analysis for the determination of the surface geometry. In the study of the integrity of nominally-stationary friction joints under cyclic loads surface modification techniques were applied. It changes the geometry of the surface layer in a wide

range of values – the roughness of a regular macro geometry of surface is changed (Fig. 3.13). It is reasonable to define the criteria that will compare the geometry of surfaces at different ways of surface modification. Laser treatment of electro-sparking coating of Cu-Mo on the base of steel C45 should be used. Creation of the reinforced surface enables to change contact stress on the spots of contact and also stiffness of surface in tangential direction. To increase the nominal fixing of contact it is necessary to decrease stiffness from one side. At the same time it is necessary to increase resistance of surface during the cyclic tangential loads.

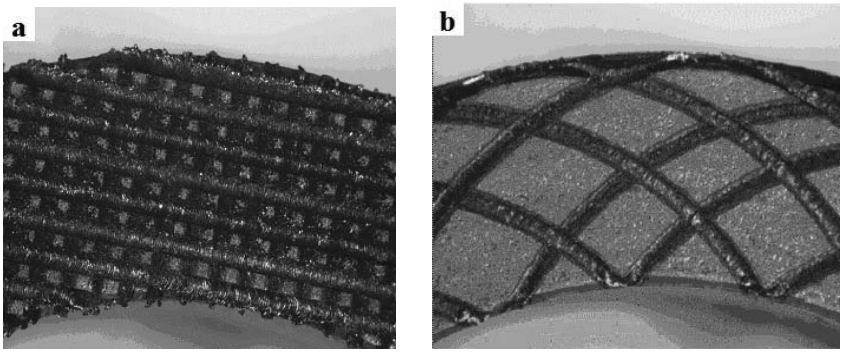

Fig. 3.13. *Coating of steel C45 by the alloy of Cu-Mo and the following impulsive laser irradiation (setting of BLS-720) hardness and a) 90% and b) 10% (x10 magnification)*

3.4.1. Integrated characteristics of a contact zone

The proposed method of surface modification is determined by the technological aspects of coatings, in particular, step and width of the modified zone. Figure 3.14 presents the dependence of tangential stiffness of contact surfaces for laser and electric-sparks treatment depending on the step of process.

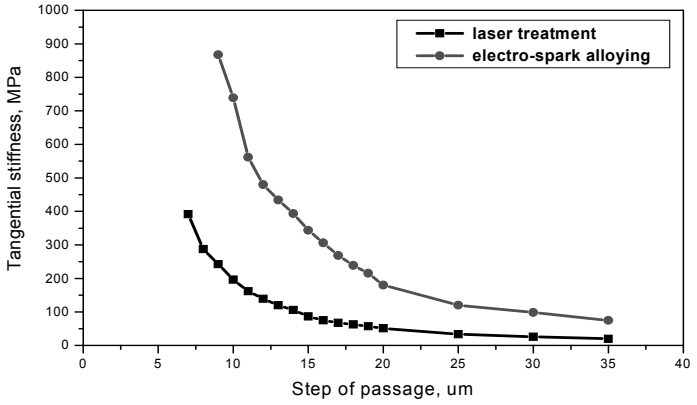

Fig. 3.14. *Dependence of tangential stiffness of contact surfaces from the step of laser treatment and electro-spark alloying*

For correct modeling of behavior of contact under conditions of alternating tangentional loading, mass characteristics of the contact zone is defined as the sum of the masses of individual elements of the model involved in contacting:

$$M = \sum_{i=1}^{N} V_i \cdot \rho = \rho \sum_{i=1}^{N} \iint_D F(x,y)dxdy \qquad (3.2)$$

where: N – number of micro contacts, ρ – density of the surface, $F(x,y)$ – function describing the surface mode of elliptic paraboloid, D – area of elements that is limited in height.

The data of mathematical modeling of contact are presented in Table 3.2.

Table 3.2. *Integrated characteristics of a contact zone for steel C45*

Type of processing	Specific value tangential stiffness, $\frac{\text{N}}{\mu\text{m}} / \text{mm}^2$		Specific mass of modified layer, $\mu g/\mu m^2$
	10 MPa	20 MPa	
Cu-Mo coating	230.52	251.489	0.19

3.4.2. Modeling of behavior of a contact zone

The complexity of surface, which has been modified, differs greatly from the characteristics of the basic material. The contact surface in the process of dynamic loading is considered to be a separate element of dynamic system (Fig. 3.15).

In this case, the mutual displacement of body 1 and body 2 $\Delta\Sigma$ can be represented as the sum of slip ΔK and deformation of the surface layer $\Delta П$ (Fig. 3.16).

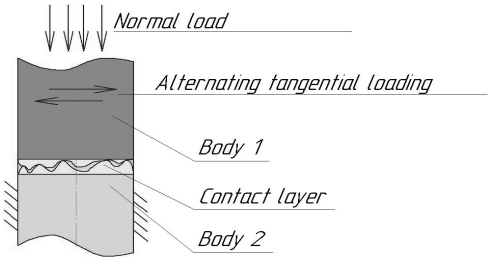

Fig. 3.15. *Representation of contact as three-component dynamical system*

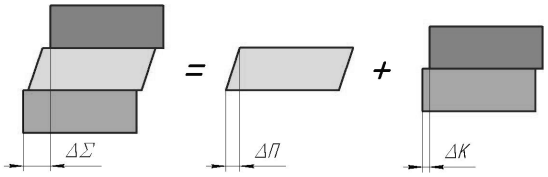

Fig. 3.16. *Scheme of distribution of the relative displacement of contact parts*

The methods of surface treatment differ greatly from the mechanical properties of the surface layers of the basic material. An important feature of the presented contact zone is selected layer, composition and specificity of any changes in the process of exploitation. From the very beginning of vibration the contact consists of microroughness of contacting bodies. With further development of fretting-wear, accumulation of wear products, surface changes its structure increasing the size of the metal layer. The dynamic motion and replacing of wear products layer finally lead to the destruction of the contact. This process is quite complex. The wear products are derived because of the low amplitude of reciprocal displacement. In general, the mass of elastically deformed layer can be represented as:

$$M = M_0 - M_{\text{det}} \tag{3.3}$$

where: M_0 – initial mass of elastically-deformed surface, M_{det} – mass of material surface, which was removed from the surface due to wear or brought out of contact.

3.4.3. Assessment of fracture process of contact, based on the concept of "third body"

In condition of nominal-fixed joints, regardless of the layer products of wear, a crucial factor for ensuring the integrity of joint is the total volume of a "third body". The effective mass of a "third body" is defined as intensity of formation in wear products:

$$M_{\text{det}} = M_{\text{stab}} + \left(M_{\text{start}} - M_{\text{stab}}\right) \cdot e^{-\left(C_S - C_W\right) \cdot \left(\frac{N}{2 \cdot \pi \cdot v}\right)} \tag{3.4}$$

where: M_{stab} – weight of wear products, C_S, C_W – factors that determine the intensity of destructive processes in the contact zone and depend on the geometrical characteristics of the surface and speed of relative motion, respectively, $M_{\max}$ – maximum amount of wear products which removes them from the contact, M_{start} – initial mass of the surface layer, v – frequency of oscillation.

Figure 3.17 shows the relationship between the mass of elastically-deformed layer to the number of loading cycles.

Modeling of work for NFJ with using the proposed method involves initial values of integral characteristics of the mass and tangentional stiffness. Mass elastically deformed layer depends on the number of loading cycles. It causes the change of dynamic properties of the contact, and therefore the system's ability to resist the tangentional displacement. Simulation results for the investigated materials are shown in Figure 3.18. Charts slip coefficient depends on the number of loading cycles for the surfaces subjected to laser exposure by capacity of 10 W and 15 W.

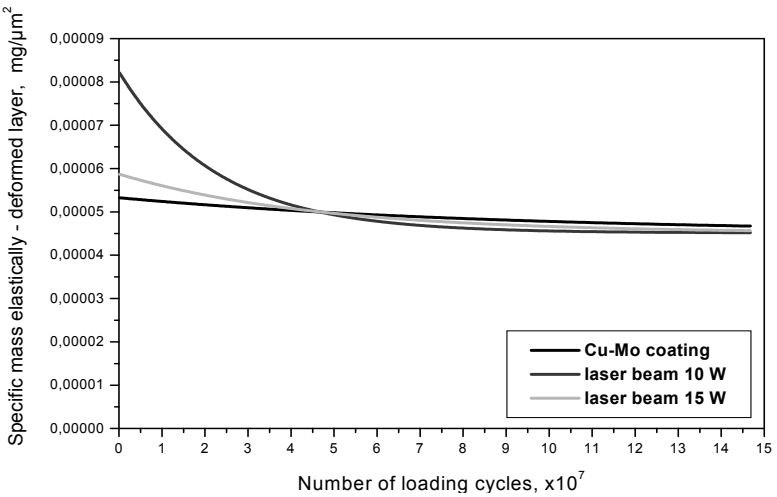

Fig. 3.17. *Dependence of mass elastically-deformed layer on the number of loading cycles*

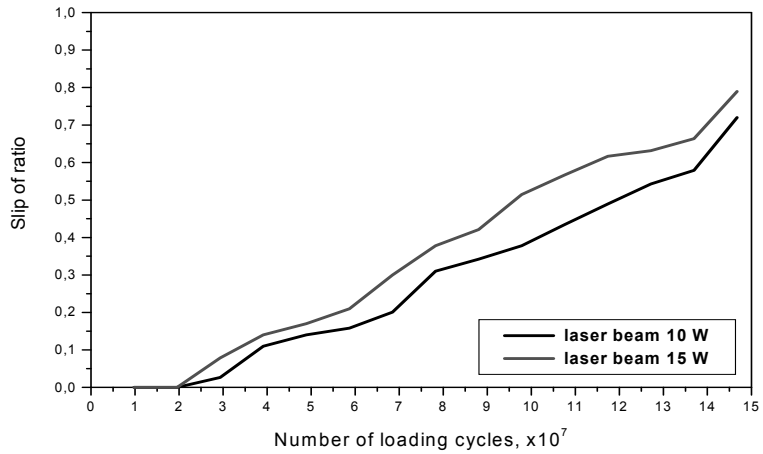

Fig. 3.18. *Simulation of dependence of the slip coefficient on the number of loading cycles for the surfaces subjected to laser exposure by capacity of 10 W and 15 W*

3.4.4. Comparison of results of numerical modeling with experimental data

Adopted mathematical model and experimental results are shown in Figures 3.19–3.26. Contact behavior under oscillation load for steel C45 after electro-spark alloying (material electrodes – Cu and Mo wires with a diameter of ∅1 mm) is presented here.

Figure 3.27 shows the graph slip of ratio which depends on the loading cycles for the experimental determination and mathematical modeling.

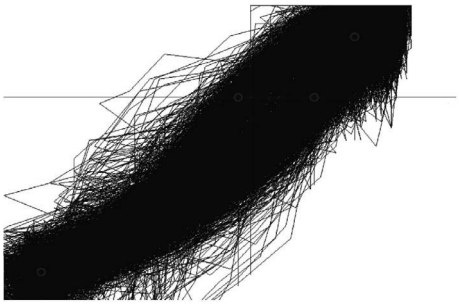

Fig. 3.19. *Results of experimental studies (number of loading cycles N = $1.5 \cdot 10^7$, amplitude of excitation A = 71.4 μm, normal load 45 N)*

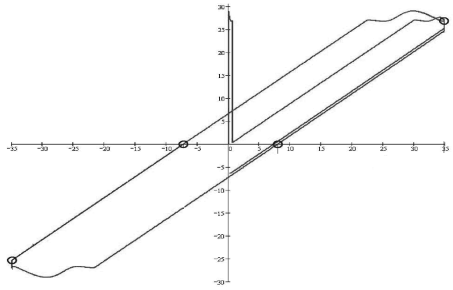

Fig. 3.20. *Results of mathematical modeling (a moving mass layer m = $8.3562 \cdot 10^{-6}$ g, stiffness system c = 230 N/μm, the amplitude of excitation A = 70 μm, normal load 45 N)*

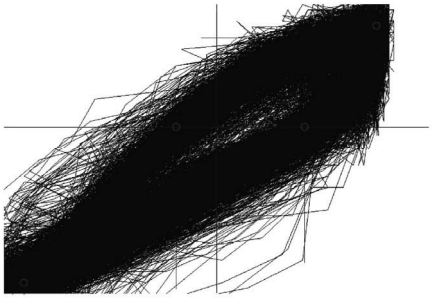

Fig. 3.21. *Results of experimental studies (number of loading cycles N = $5 \cdot 10^7$, amplitude of excitation A = 73.5 μm, normal load 45 N)*

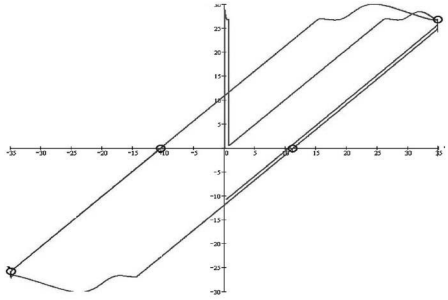

Fig. 3.22. *Results of mathematical modeling (a moving mass layer m = $1.3895 \cdot 10^{-6}$ g, stiffness system c = 230 N/μm, the amplitude of excitation A = 70 μm, normal load 45 N)*

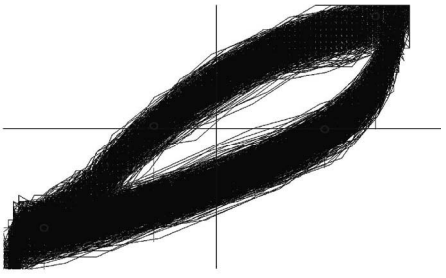

Fig. 3.23. *Results of experimental studies (number of loading cycles N = 10^8, amplitude of excitation A = 74.6 μm, normal load 45 N)*

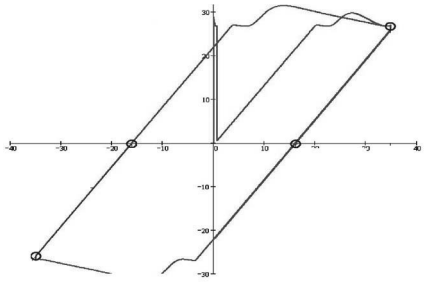

Fig. 3.24. *Results of mathematical modeling (a moving mass layer m = $0.425 \cdot 10^{-6}$ g, stiffness system c = 230 N/μm, the amplitude of excitation A = 75 μm, normal load 45 N)*

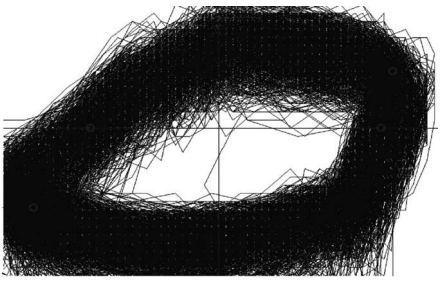

Fig. 3.25. *Results of experimental studies (number of loading cycles N = $1.5 \cdot 10^8$, amplitude of excitation A = 75.21 μm, normal load 45 N)*

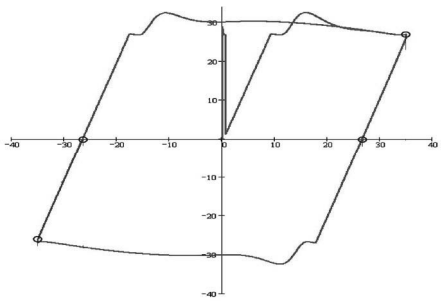

Fig. 3.26. *Results of mathematical modeling (a moving mass layer m = $0.273 \cdot 10^{-6}$ g, stiffness system c = 230 N/μm, the amplitude of excitation A = 75 μm, normal load 45 N)*

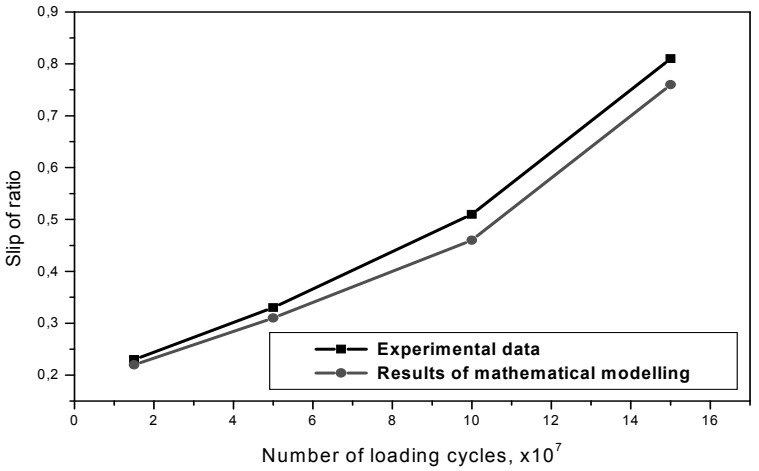

Fig. 3.27. *Comparison of experimental and mathematical modeling of behavior of nominally-fixed contact at treatment by electro-spark alloying*

Thus the proposed method evaluates the influence of surface modification methods by creating a regular relief on the surfaces of nominally-fixed friction joints in long-term ability to maintain the integrity of contact under vibration loads.

The hardness of the cell after the laser treating was measured in percents, as relation of area treated by the laser irradiation to the unit of area without treatment. In Figure 3.13 surfaces are shown after reinforcing by the laser irradiation of coating of Cu-Mo from 10% and 90% to the hardness of treatment.

Comparative description of vibroactivity of contact pair of harden steel C45 and steel C45 + Cu-Mo + laser irradiation which depends on the hardness of laser treatment and normal pressure is shown in Figure 3.28.

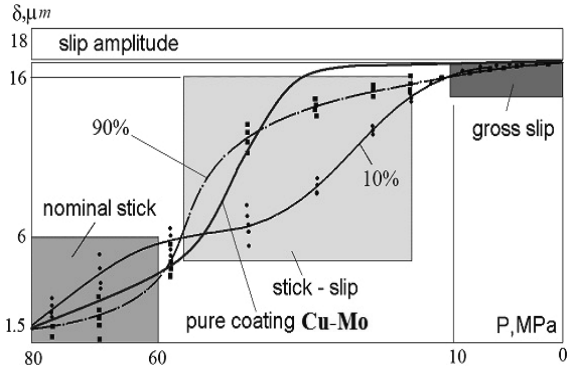

Fig. 3.28. *Evolution of microdisplacement of contact pair depending on the normal pressure and the hardness of treatment. Frequency of oscillation 50 Hz, final amplitude 18…20 μm*

During the cyclic loading due to the wear the normal pressure in an interface is lowered to zero. The slip amplitude is multiplied at the same time. These two criteria determine the fretting resistance of the contact surfaces. It is necessary to point out that the duration of the tests is equal to 200…300 hours of continuous oscillation.

Thus it is possible to draw the following conclusions. The least cells appeared by the laser irradiation on coating is effective at large stress and provide the mixed contact without global slipping. The increase of sizes of cell is advantageous for stick-slip regime. The concentration of normal force on the height roughness creates effective tangential stiffness and sticking of surfaces. After the laser reinforcing such type of roughness, which allows to accumulate products of fretting in hollow of separate cells and simultaneously to keep a high level adhesive and metallic joints on the spots of contact is created. It also promotes the sticking of surfaces. In general, reinforcing of electro-sparks coating by the laser irradiation influences the contact pressure. It leads to the decrease of vibration activity of contact pair to 30% in the regime of long duration of small amplitude fretting.

3.5. TEXTURE IMPACT ON CONTACT ISSUES

Frictional resistance between slide rings of the end-face seal depend on interrelations between elementary processes that occur in the gap. The processes include the following: hydrostatic and hydrodynamic action of the medium, the medium adhesion to the substrate, change in the gap geometry due to thermal and mechanical deformation, carrying away of heat, changes of phase and rheological properties of the liquid in the gap. Those interrelations, in turn, cannot be considered without referring to the physical properties of the medium, and of the surfaces that enclose the gap (e.g. viscosity, wettability), or to kinematic and dynamic relations between the above-mentioned factors. It should be understood that, depending on the factors, those elementary interrelations can produce either

synergistic or antagonistic effect on the minimisation of frictional resistances in the seal gap. Bearing that in mind, the role of macro- and micro-geometry of the surfaces that constitute the gap needs to be taken into account. Departure from smooth and flat surface, if regular in character and properly designed, can bring about synergistic effect on the desirable properties of a sliding pair, such as bearing, durability and reliability. In view of all the arguments above, an important role for surface engineering technologies in producing sliding friction pairs should be emphasised. Those technologies, which once contributed to the manufacturing of flat and smooth surfaces, are currently employed to make heterogeneous and textured surfaces [74–77].

Figures 3.29 and 3.30 show examples of heterogeneous surfaces.

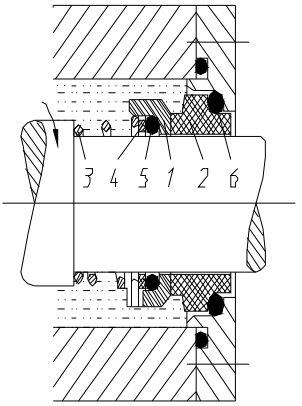

Fig. 3.29. *Schematic diagram of the face seal: 1 – axially shifted sliding ring, 2 – anti-ring, 3 – spring, 4 – clamping ring, 5, 6 – secondary seals [74]*

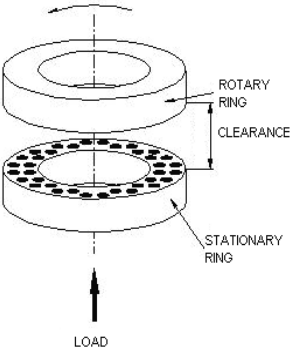

Fig. 3.30. *Model of sliding pair with textured surface [74]*

Generally, the real contact surface is smaller than the nominal one and contact load onto real contact surfaces are higher than the corresponding nominal values. In particular, while analysing the real geometries of contact of geometrically textured surfaces, it is necessary to have data on the real contact surface.

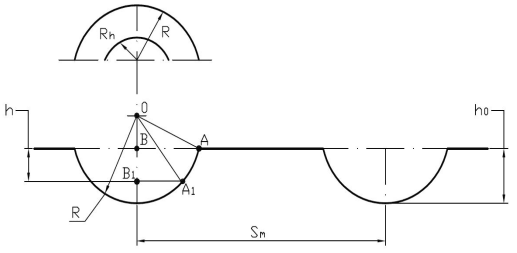

Fig. 3.31. *Diagram of a geometric texture with spherical dimples*

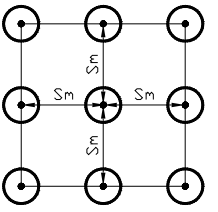

Fig. 3.32. *Dimple spacing in the surface with uniform texture*

Depending on load, and also due to wear, the surface bearing profile undergoes changes. The analysis of changes in the bearing surface for the shape profile with spherical dimples is presented above (Fig. 3.31 and 3.32). As a result of deformations caused by load or wear, the depth of dimples of h values is reduced in service, which also produces a reduction in the dimple radius to the value of R_h.

$$R_h = A_1B_1 = \sqrt{R^2 - (R - h_0 + h)} = \sqrt{(h_0 - h)(2R - h_0 + h)} \tag{3.5}$$

For $2R >> h$

$$R_h = A_1B_2 = (R - h_0)^{\frac{1}{2}}(h_0 - h)^{\frac{1}{2}} \tag{3.6}$$

Because of exploitation, the bearing surface α (the ratio of the surface without dimples to the nominal surface) will be changed to the value of α_h:

$$\alpha = \frac{A_n}{A_0}, \quad \alpha_h = \frac{A_h}{A_0} \tag{3.7}$$

where: $A_n = A_0 - k\pi R^2$, $A_h = A_0 - k\pi R_h^2$ (k – number of dimples on the surface A_0).

If loading with F force is assumed, the following dependence for the value of pressure on the surface is received:

$$\sigma_h = \frac{F}{A_h}, \ \sigma_0 = \frac{F}{A_0} \tag{3.8}$$

After substituting dependences (3.6) and (3.7), the following is obtained:

$$\sigma_h = \left(\frac{A_0}{A_0 - k\pi(R - h_0)(h_0 - h)} \right) \sigma_0 \tag{3.9}$$

The amount of lubricant, its distribution and properties create various situations in the sliding pair. Those generate processes in the contact zone, which are different qualitatively and quantitatively. If only the amount and wetting properties of the lubricant are taken into account, four cases should be differentiated (Fig. 3.33).

Texture is described by geometric relations for a single texture element, and also by relations that refer to their spacing on the friction surface. As regards a texture composed of uniformly distributed dimples having the form of spherical bowls, it is possible to state relations between a degree of blackening, diameter and depth of dimples and their volume.

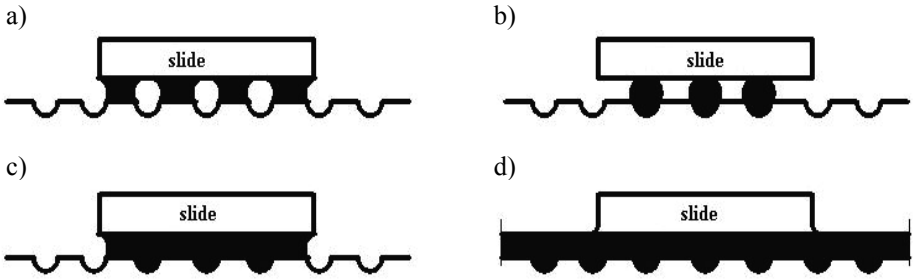

Fig. 3.33. *The interaction of the lubricant and the textured surface in the sliding pair: a) lean lubrication with a weak wetting agent, b) lean lubrication with a good wetting agent, c) sufficient lubrication of the slide with a good wetting agent, d) abundant and continuous lubrication of the textured surface*

3.5.1. Texturing methodology and wear tests

Laser surface texturing is one of the most common and promising methods of surface roughening. Categorized as a metal removal process, laser texturing is usually performed at a power density of 10^6–10^9 W/cm^2. At present, it accounts for about 2% of all laser-based material processing processes used in the world.

In laser surface texturing, a pulsed laser beam is focused on a material to melt a hole. The hole depth is dependent mainly on the power density and the pulse duration. The drilling debris is removed from a hole being drilled using compressed air or another inert gas.

The tests were conducted for Cu-Mo coatings produced by electro-spark deposition onto rings made of carbon steel C45.

The texturing was performed using an Nd:YAG laser (impulse mode), model BLS 720, and operating in the pulse mode under the following conditions:

- laser spot diameter, d = 0.7 mm
- laser power, P = 20 W
- beam shift rate, v = 1200 mm/min
- nozzle-sample distance, h = 1 mm
- pulse duration, t_i = 1.2 ms
- frequency, f = 8 Hz.

A Joel JSM-5400 scanning electron microscope was used to study the effects of laser surface texturing. Selected SEM images are presented in Figures 3.34 and 3.35. As can be seen, the surface structure after laser surface texturing is regular. The surface is covered by bumps and dimples resulting from phase and structural modifications and the accompanying specific volume changes in the laser affected zones. Lapping and super finish are used to obtain hard flat areas transferring normal loads and areas of pores where the hydrodynamic forces are generated during fluid lubrication. Surfaces with such a texture can be applied, for instance, to sliding friction systems. The microscopic analysis showed that the removal of the drilling debris was not complete when the laser beam was focused locally. This

was probably due to insufficient power density. The action of the thermocapillary forces and the convective motion resulted in the formation of rims, whose structure consisted of molten and then crystallized Cu-Mo.

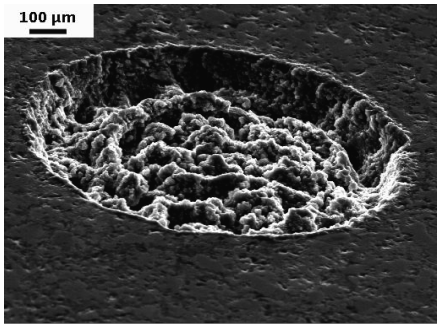

***Fig. 3.34**. A single microcavity on the ring*

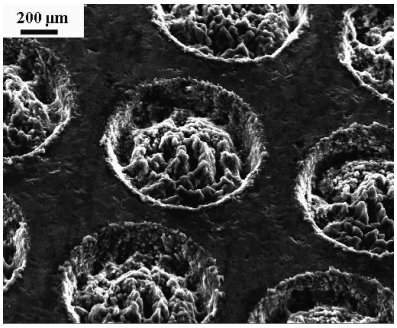

***Fig. 3.35.** A system of microcavities on the ring*

The wear tests of the Cu-Mo electro-spark deposited coatings before and after laser surface texturing were carried out using the pin-on-disc tester T-01M.

The tester makes it possible to measure the friction force for a predetermined load. The pin ∅4 mm x 20 mm was made of tool steel. The samples and anti-samples were prepared in accordance with the instruction. The tests were conducted at the following parameters of friction:

- linear velocity, $v = 0.8$ m/s
- test duration, $t = 3600$ s
- sliding distance, $S = 2880$ m
- range of load changes: 5, 10, 15 N.

A drop of lubricant – paraffin oil was applied on the ring raceway only once. It was necessary to measure the time after which the value of the friction coefficient increased.

The wear test results for the electro-spark deposited Cu-Mo coating before and after laser surface texturing are shown in Tables 3.3 and 3.4.

***Table 3.3.** Results of the wear test for the Cu-Mo coating after laser surface texturing*

Load, N	**Mass loss, mg**			
	not lubricated		lubricated oil	
	pin	disc	pin	disc
5	5.44	6.88	3.35	4.26
10	10.24	12.16	7.11	8.63
15	14.88	20.16	10.29	15.72

Table 3.4. *Results of the wear test for the Cu-Mo coating before laser surface texturing*

Load, N	**Mass loss, mg**			
	not lubricated		lubricated oil	
	pin	disc	pin	disc
5	6.16	9.64	4.89	6.33
10	13.05	16.84	9.06	11.54
15	19.41	23.28	13.14	18.67

Table 3.5 shows the values of the friction coefficient for the Cu-Mo coating before and after laser surface texturing.

Table 3.5. *Results of the friction coefficient for the Cu-Mo coating before and after laser surface texturing*

Load, N	**Friction coefficient**			
	not lubricated		lubricated oil	
	Cu-Mo	CuMo+laser	Cu-Mo	Cu-Mo+laser
5	0.39	0.40	0.21	0.14
10	0.54	0.46	0.35	0.23
15	0.67	0.48	0.43	0.32

Conclusions:

1. It is possible to diversify the surface of electro-spark deposited coatings, i.e. to obtain heterogeneous surfaces. The laser-affected areas are characterized by the occurrence of regular cavities, hardened areas and varied roughness.
2. The surface heterogeneity (i.e. the cavities) is desirable in sliding friction pairs. They may be used as reservoirs of lubricants as well as sources of hydrodynamic forces increasing the capacity of a sliding pair.
3. A concentrated laser beam can effectively modify the state of the surface layer, i.e. the functional properties of electro-spark coatings can be achieved.
4. There is no change in the chemical composition of electro-spark deposited coatings after laser treatment The results of laser radiation are the homogenization of the chemical composition, structure refinement and the healing of microcracks and pores.
5. An effective way to increase a long-term integrity of NFJ for structural steels and alloys are developed by combined surface treatment – electro-spark alloying by hard alloys, followed by laser irradiation. The corresponding

density of laser irradiated surface created cell sizes, which led to the reinforcement. Depending on external factors and the dynamic conditions of contact the power density of laser radiation was chosen to provide several options for modifying surfaces: surface asperities melting, homogenization or deep remelting together with the base. The thickness of modified layer does not exceed 10 microns. This treatment leads to reduce of vibration activity of activity NJF on 35...50% and increase of fretting – resistance of contact on 1.5...4 times. The thickness of modified layer does not exceed 10 microns.

In the next phase of the research, it is essential to determine the phase composition and porosity of the coatings before and after laser treatment.

The future investigations will be continued in direction for development better heterogonous surface for tribological applications by using ESD technique.

4. LASER TREATMENT OF FLAME AND PLASMA SPRAYED COATINGS

4.1. INTRODUCTION

Wear and abrasion are serious problems in all branches of industry. Although modern technologies permit considerable improvement of properties of the outer layer, they need to be modified or new solutions have to be looked for [78, 79]. Laser treatment is one of the technologies that allows shaping of the outer layer. An increased interest in its utilisation is due to the specific properties of laser radiation. As it is possible to construct radiation sources with appropriate parameters, such as wavelength, lateral beam mode, emission power, impulse energy, impulse duration, etc., lasers are being more and more frequently applied to various tasks. This is possible because the investigations into the utilisation of laser technologies are being carried out on a large scale now. As a result, a number of laser-based systems have been constructed and produced. In spite of the fact that the laser was invented 52 years ago and a great deal has been achieved in this field since then, its application to surfacing is still negligible. This is mainly owing to high costs of laser systems. Moreover, researchers find it difficult to develop technologies that would take into account the absorption of a laser beam by the surface [80]. Industry makes use of gas lasers (CO_2) and lasers on a solid (Nd:YAG). Their applicability results from the parameters characterising these lasers: power, quality of the emitted beam and efficiency. The number of excimer and the recently developed semi-conductor lasers used in industry is still very small (less than several per cent). Of particular significance is the applicability of laser treatment to improve the properties of thermally sprayed coatings. It is possible to obtain coatings with no, or small porosity, higher hardness and resistance to wear, corrosion, oxidation, etc. [81–83].

4.2. EXPERIMENTAL

Typical commercial Ni-based powder materials for flame and plasma spraying were used: NiAl (Amdry 956), NiCr (Amdry 4535) and NiCrAlMoFe (Amil AMI 3464). The particle size and shape of the powders are shown in Figure 4.1. The chemical composition of powders as well as the granulation of particles are shown in Table 4.1.

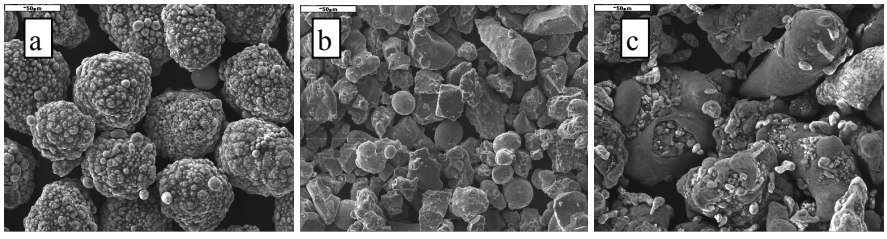

Fig. 4.1. *NiAl (a) NiCr (b) NiCrAlMoFe (c) powders*

Table 4.1. *Particle size and chemical composition of the experimental powders*

Powder specification	Particle size, μm	Chemical composition, % wt.				
		Ni	Cr	Al	Mo	Fe
AMDRY 956	–90 + 45	95	–	5	–	–
AMDRY 4535	–53 + 16	80	20	–	–	–
AMIL 3464	–125 + 45	73.5	9	7	5.5	5

Samples measuring 30 mm x 30 m x 3 mm made of low-carbon steel were coated and grit blasted with 12 grade electrocorundum at a pressure of 0.5 MPa. A Castolin Rotoloy gun was used for flame spraying, whereas plasma spraying was carried out using a plasma set Plancer, equipped with a gun PN120 and powder feeder Thermal Miller 1260. Argon plasma with 7% hydrogen addition was used. The applied flame and plasma spraying parameters are presented in Table 4.2. The thickness of coatings after spraying was 0.6–0.7 mm.

Table 4.2. *Spraying parameters*

Flame	**Plasma**
Acetylene (MPa) 0.07	Arc current (A) 450
Oxygen (MPa) 0.4	Voltage (V) 50
Powder flow rate (g/min) 70	Powder flow rate (g/min) 65
Spraying distance (mm) 200	Spraying distance (mm) 130

A CO_2 TLF 6000 TURBO laser operating in the continuous mode was applied to remelt thermally sprayed coatings. The laser makes it possible to focus energy reaching $7 \cdot 10^7$ W/cm^2. The parameters characterising the laser are: wavelength $\lambda = 10.6$ μm, efficiency $\eta = 7\%$, maximum power $P = 6000$ W. Preliminary testing involved selecting the parameters of laser remelting for the coated samples. This required considering the power and speed of a laser beam as well as the distance of the lens focus from the surface being machined. The following machining parameters were us:

- laser power, $P = 800$; 1000; 1200 and 1400 W
- laser beam speed, $v = 1000$ mm/min
- distance from focus, $\Delta f = 40$ mm.

Unfinished coatings were subjected to laser treatment using a round cross-section of the beam. Resistance to abrasive wear was tested using a tribological instrument T-07, whose diagram is presented in Figure 4.2.

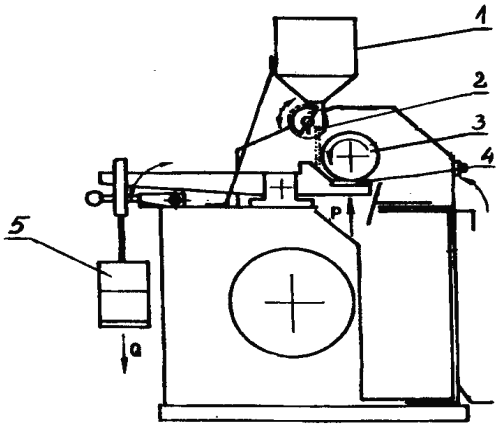

Fig. 4.2. *Tribological tester T-07: 1 – container, 2 – abradant, 3 – antisample, 4 – sample, 5 – load*

The abrasive material, i.e. electrocorundum EB-90, was supplied by the feeder in between the rotating rubber roller and the coated sample. Mass decrement was measured after 10, 20 and 30 minutes. A standard test was applied. The microstructure of the sprayed coatings was analysed with an optical microscope Epityp 2 and a scanning electron microscope JOEL JSM-5400. The distribution of elements was studied by means of a microprobe ISIS 300 Oxford Instruments. The microhardness of coatings was measured by means of the Vickers method using a load of 0.98 N.

4.3. RESULTS

4.3.1. Microstructure of coatings

The microstructure of flame and plasma sprayed coatings is shown in Figures 4.3 and 4.4. In all cases, we can observe a lamellar structure, which is typical of thermally sprayed coatings. The morphology of flame sprayed coatings demonstrates that the particles are considerably less deformed as compared with those of plasma sprayed coatings and that some powder particles have not been melted. The structures of plasma sprayed coatings illustrated in Figure 4.4 are more homogeneous, which is a result of the exposure to a high temperature and great plasma velocity.

Plasma sprayed coatings are characterised by lower porosity than the flame sprayed coatings. The morphology is completely different, however, if a laser beam is applied. It depends mainly on the laser treatment parameters. Figure 4.5 shows examples of the structure of coating surfaces subjected to laser machining. It was established that the structure of the outer layer of the as-sprayed coating and its phase composition influenced the absorption of the laser beam. Flame sprayed coatings were more absorptive than plasma sprayed coatings. For each material, the

surface image was different, although the same parameters of laser treatment were applied. It was found that a NiCrAlMoFe coating had the greatest absorptivity, while a NiAl had the smallest. In the case of a NiCr coating, the applied power (1000, 1200 and 1400 W) caused intensive remelting of coatings, and in consequence, formation of pores and cracks in the remelted layer and spheroidal separations on the surface (Fig. 4.5).

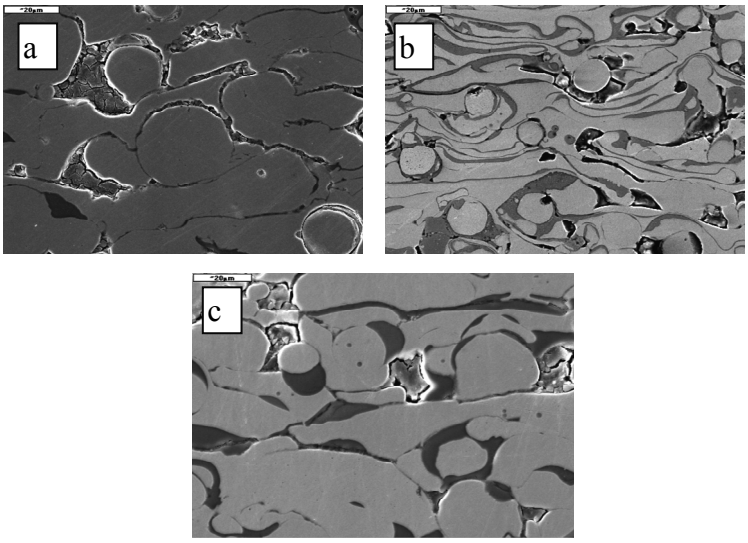

Fig. 4.3. *Flame sprayed coatings: NiAl (a) NiCr (b) NiCrAlMoFe (c)*

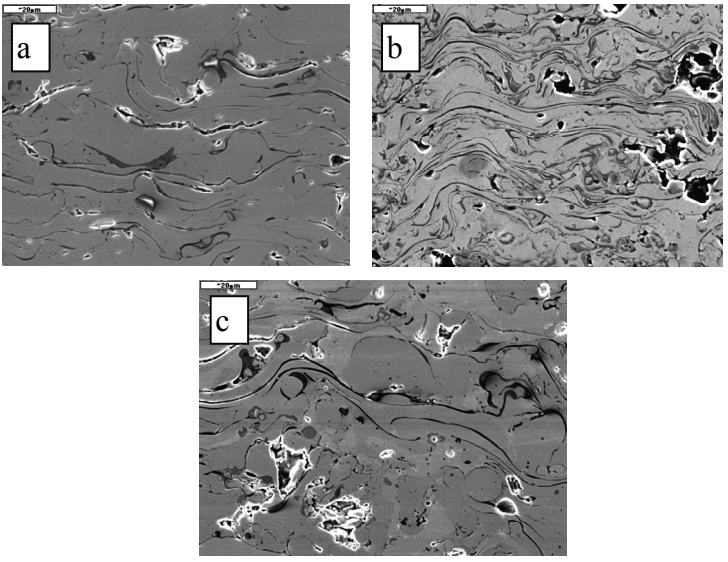

Fig. 4.4. *Plasma sprayed coatings: NiAl (a) NiCr (b) NiCrAlMoFe (c)*

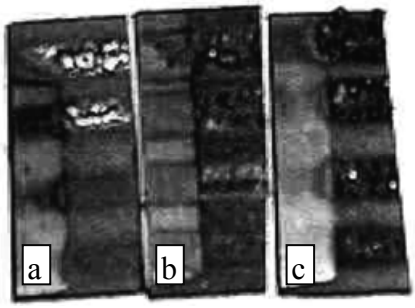

Fig. 4.5. *Flame sprayed coating after laser treatment: NiAl (a) NiCr (b) NiCrAlMoFe (c)*

Uniform remelting of the coating could be observed on the surface of samples when a power of 800 W was applied. It was confirmed on metallographic specimens of the coating remelted zone (Figs. 4.6a and 4.7a).

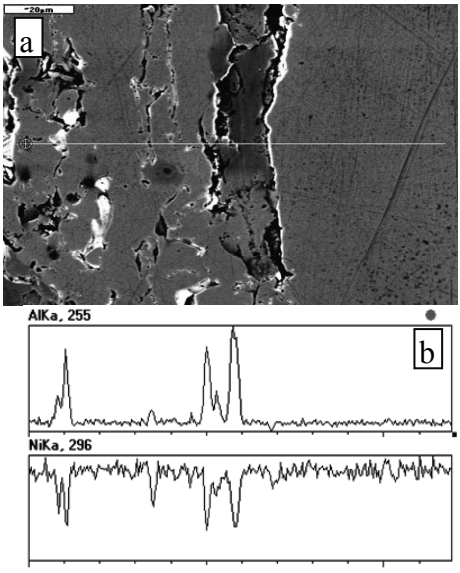

Fig. 4.6. *Remelted zone of plasma sprayed NiAl coating (a) distribution of elements in the transition zone (b)*

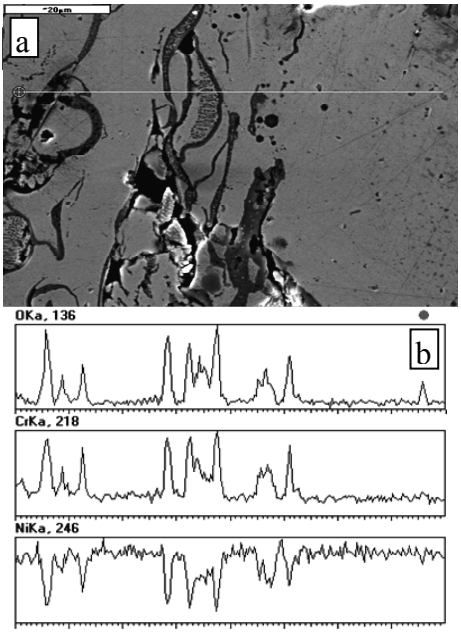

Fig. 4.7. *Remelted zone of flame sprayed NiCr coating (a) distribution of elements in the transition zone (b)*

One can observe a clear transition from a lamellar structure with considerable porosity into a completely remelted zone characterised by lack of porosity. The study of chemical composition distribution (Figs 4.6b and 4.7b) testifies to high homogeneity of the structure obtained by laser remelting. In the case of sprayed NiAl coatings, the remelting occurred only when a power of 1200 W was applied. At 1000 and 1200 W, the remelted coating did not contain any spheroidal separations, nor

was it porous in the zone subjected to laser treatment. The analysis of chemical composition proved that a material with a homogeneous structure had been formed.

4.3.2. Microhardness of coatings

The application of the laser to treatment of coatings caused changes in their microhardness. The changes in hardness in the function of distance from the surface depend on the value of power applied, type of material and spraying technique. The higher the value of the laser power, the higher the hardness of coatings. The application of the lowest power, i.e. 800 W, resulted in a slight increase in hardness from 175 HV0.1 to 235 HV0.1, while a power of 1200 W made it possible to obtain hardness of 350 HV0.1. In the case of a plasma-sprayed NiCrAlMoFe coating, its decrease at a depth of 200 μm and power of 1200 W and 1400 W is related to the formation of a porous structure with internal microcracks resulting from laser treatment. Coatings machined at lower powers of a laser beam, i.e. 800 W and 1000 W do not demonstrate such a decrease in microhardness.

4.3.3. Wear resistance

The results of wear resistance of flame and plasma sprayed coatings are presented in Figure 4.8a. The highest resistance to wear was demonstrated by a plasma sprayed NiCrAlMoFe coating and the lowest by a flame sprayed NiCr coating. The experiments have provided evidence that plasma sprayed coatings were slightly more resistant to wear than flame sprayed ones.

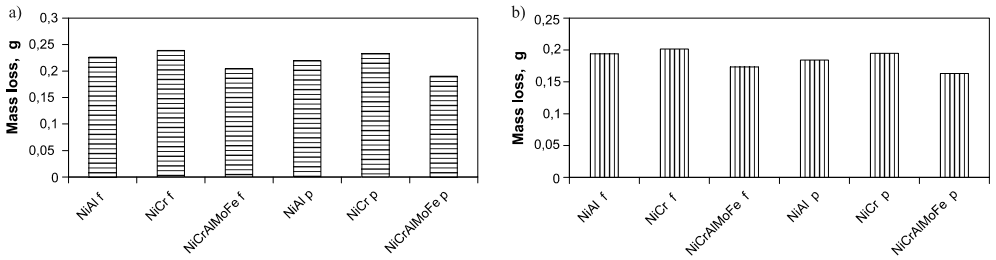

Fig. 4.8. *Wear resistance of coatings: as sprayed (a) after laser treatment (b)*

To test the wear resistance of coatings after laser treatment, samples with uniformly remelted outer layer containing the smallest number of separations, pores and microcracks were selected so that measuring results would not be influenced by them. The results of the testing of wear resistance of such coatings are shown in Figure 4.8b. The wear of coatings after laser treatment is smaller as compared to non-machined coatings. The differences in the wear resistance between flame and plasma sprayed coatings decreased as well. Yet, a plasma sprayed NiCrAlMoFe coating remelted with a laser beam at a power of 1000 W demonstrated the highest resistance to wear.

Conclusions

The results of the study concerning the laser processing of flame and plasma sprayed coatings indicate that:

1. The rates of surface remelting differed depending on the laser processing parameters, particularly the power of the laser beam; the highest rate of surface remelting was reported at P = 1400 W, while the lowest was obtained at P = 800 W.
2. The absorption of laser radiation, which had a considerable influence on the rate of surface remelting, was dependent on the coating material and the spray method.
3. The absorption capacity of the flame sprayed coatings was higher than that of the plasma sprayed coatings; the absorption of laser radiation was the highest for the NiCrAlMoFe coatings and the lowest for the NiAl coatings.
4. Laser processing contributed to an increase in the microhardness of all the coatings; of significance were the following parameters: power of the laser beam, type of the coating material and the spray method.
5. The laser-remelted coatings had higher abrasive wear resistance than the surfaces not modified with laser, i.e. flame or plasma-sprayed coatings.

References

[1] Ho K.H., Newman S.T.: *State of the art electrical discharge machining*. International Journal of Machine Tools & Manufacture, 43 (2003), pp. 1287–1300.

[2] Miernikiewicz A.: *The bases of experimental and theoretical in electro discharge machining (EDM).* Technical University of Cracow, 274 (1999).

[3] DiBitonto D.D., Eubank P.T., Patel M.R., Barrufet M.A.: *Theoretical models of the electrical discharge machining process. I-A simple cathode erosion model*. Journal of Applied Physics 66, 9 (1989), pp. 123–131.

[4] Spadło S. et al.: *Investigation of electro-discharge mechanical dressing (EDMD) of diamond abrasive wheels with conductive bonds using brush electrodes*. Journal Engineering Manufacture, Vol. 219, part B, (2005), pp. 1–8.

[5] Ribalko A.V., Sahin O.: *The use of bipolar current pulses in electro-spark alloying of metal surfaces.* Surface & Coatings Technology, 168 (2003), pp. 129–135.

[6] Galinov I.V., Luban R.B.: *Mass transfer trends during electrospark alloying*. Surface & Coatings Technology, 79 (1996), pp. 9–18.

[7] Ozimina D., Scholl H., Styp-Rekowski M.: *Formowanie przeciwzużyciowych warstw wierzchnich obróbką elektroiskrową. Wybrane zagadnienia obróbek skoncentrowaną wiązką energii*, rozdział 2, 2003, s. 104–109.

[8] Radek N., Wrzałka Z., Szalapko J.: *Measurement of electric impulses and properties of carbides electro-spark coatings*. [in:] *Scientific basis of modern technologies*: *experience and prospects*. ed. by J.I. Shalapko and L.A. Dobrzański, Jaremche 2011, Ukraine, pp. 223–235.

[9] Radek N., Wrzałka Z., Szalapko J., Bronček J.: *Struktura geometryczna powierzchni i własności tribologiczne przeciwzużyciowych powłok elektroiskrowych* [w:] *Inżynieria Powierzchni wybrane zagadnienia*. Red. Bogdan Antoszewski, Wydawnictwo Politechniki Świętokrzyskiej, Kielce 2011, s. 132–139.

[10] U.S. Patent No. 5071059 Method for joining single crystal turbine blade halves – 1991.

[11] http:// www.stt-inc.com

[12] G.B. Patent No. 637793 A metod of working Metals – 1946.

[13] DiBitonto D.D., Eubank P.T., Patel M.R., Barrufet M.A.: *Theoretical models of the electrical discharge machining process. I-A simple cathode erosion model.* Journal of Applied Physics, 66/9 (1989), pp. 123–131.

[14] Zolotych B.N.: *Osnovnyje voprosy kaciestviennoj teorii elektroiskrovoj obrabotki v zidkoj dielektricieskoj srede. Problemy elektrićeskoj obrabotki metallov*. Moskwa 1962.

[15] Petrow J. (red.): *Elektroiskrowoje legirowanie metallićieskich powierchnostoj*. Kisziniew 1985.

[16] Abu Zeid O.A.: *On the effect of electrodischarge machining parameters on the fatigue life of AISI D6 tool steel.* Journal of Materials Processing Technology, 68, 1 (1997), pp. 27–32.

[17] Lazarenko B.R., Lazarenko N.I.: *Elektroiskrovaja obrabotka tokoprovodiaszćih materiałow.* Akademia Nauk CCCP, Moskwa 1958.

[18] Galinov I.V., Luban R.B.: *Mass transfer trends during electrospark alloying*. Surface and Coatings Technology, 79 (1996), pp. 9–18.

[19] Samsonow G., Wierhotyrow A., Bowkun G., Sycziew B.: *Elektroiskrowoje legirowanie metalliczeskich powierchnostoj.* Wydawnictwo Naukowa Dumka, Kijev 1976.

[20] Pierzynowski R.: *Badania elektroiskrowego stopowania powierzchni elektrodami szczotkowymi*. Rozprawa doktorska, PW, Warszawa 2001.

[21] Wierhotyrow A.D., Mulin J.I., Astapowa E.S., Agapiatow W.A., Cietinin M.I., Kozyr A.W., Sołowiew W.W.: *Wlijanie riezimow eliektroiskrowogo liegirowanija i eliektrodnych materiałow na struktury i iznosostoikost pokrytij*. Elektronnaja Obrabotka Materiałow, 3 (2004), s. 21–25.

[22] Konstanty J.: *Powder metallurgy diamond tools*. Elsevier, Oxford 2005.

[23] Hebda M., Wachal A.: *Trybologia.* Wydawnictwo Naukowo-Techniczne, Warszawa 1980.

[24] Kupczyk M.: *Jakość technologiczna i użytkowa ostrzy skrawających z powłokami przeciwzużyciowymi*. Politechnika Poznańska – Rozprawy, 320, Poznań 1997.

[25] Dobrzański L.A.: *Podstawy nauki o materiałach i metaloznawstwo*. Wydawnictwo Naukowo-Techniczne, Warszawa 2002.

[26] Wrzałka Z., Radek N.: *Pomiary i analiza impulsów elektrycznych podczas obróbki elektroiskrowej.* Zeszyty Naukowe Politechniki Świętokrzyskiej – Terotechnologia 2008, Budowa i Eksploatacja Maszyn, 11 (2008), s. 329–336.

[27] Radek N.: *Determining the operational properties of steel beaters after electrospark deposition*. "Eksploatacja i Niezawodność – Maintenance and Reliability", 4 (2009), pp. 10–16.

[28] Radek N., Broncek J.: *Tribological properties of anti-wear carbides coatings*. Technolog, 6 (2009), pp. 56–59.

[29] Chang-bin T., Dao-xin L., Zhan W., Yang G.: *Electro-spark alloying using graphite electrode on titanium alloy surface for biomedical applications.* Applied Surface Science, 257 (2011), pp. 6364–6371.

[30] Radek N., Bartkowiak K.: *Performance properties of electro-spark deposited carbide-ceramic coatings modified by laser beam*. Physics Procedia, 5 (2010), pp. 417–423.

[31] Radek N., Bartkowiak K.: *Laser treatment of Cu-Mo electro-spark deposited coatings*. Physics Procedia, 12 (2011), pp. 499–505.

[32] Radek N., Wajs W., Luchka M.: *The WC-Co electrospark alloying coatings modified by laser treatment.* "Powder Metallurgy and Metal Ceramics", 3–4/2008, pp. 197–201.

[33] Radek N., Antoszewski B.: *Influence of laser treatment on the properties of electro-spark deposited coatings*. Kovove Materialy-Metallic Materials, 1 (2009), pp. 31–38.

[34] Burakowski T., Wierzchoń T.: *Inżynieria powierzchni metali*. Wydawnictwo Naukowo-Techniczne, Warszawa 1995.

[35] Domański R.: *Promieniowanie laserowe – oddziaływanie na ciała stałe*. Wydawnictwo Naukowo-Techniczne, Warszawa 1990.

[36] Domański R., Jaworski M.: Oddziaływanie impulsów laserowych na ciała stałe z pokryciami o mikronowych grubościach. Archiwum Termodynamiki, vol. 10, 1–2 (1989), s. 97–114.

[37] Kusiński J.: *Lasery i ich zastosowanie w inżynierii materiałowej*. Wydawnictwo Naukowe Akapit, Kraków 2000.

[38] Moriya N.: Granulating apparatus. US Patent 4,655,701 (April 7, 1987).

[39] Weber G.: *Granulating: a new process for diamond tool producers.* In Proceedings of International Workshop on Diamond Tool Production, Turin, Italy, November 8–10, 1999, pp. 73–82.

[40] Baert M.: *Coating of diamonds and granulation of metal powders.* In Proceedings of Seminar on PM Diamond Tools, Lausanne, Switzerland, November 2–3 (1995), pp. 24–40.

[41] Van Doorslaer T.: *Coating of abrasive grains and the granulation of metal powders.* In Proceedings of International Workshop on Diamond Tool Production, Turin, Italy, November 8–10 (1999), pp. 83–88.

[42] Burckhardt S.: *New technique for granulating diamond and metal powders.* Industrial Diamond Review 57, 4 (1997), pp. 121–122.

[43] Weber K.: *Modern diamond segment production on cold presses and hot presses.* In Proceedings of Seminar on PM Diamond Tools, Lausanne, Switzerland, November 2–3 (1995), pp. 48–50.

[44] Weber G., Burckhardt S.: *Economic production of diamond segments.* Industrial Diamond Review 58, 4 (1998), pp. 111–112.

[45] Anon.: *New high-performance cold press from Dr Fritsch*. Industrial Diamond Review 63, 4 (2003), p. 25.

[46] Adamczak S.: *Pomiary geometryczne powierzchni. Zarysy kształtu, falistości i chropowatości*. Wydawnictwo Naukowo-Techniczne, Warszawa 2008.

[47] Adamczak S.: *Normalizacja pomiarów struktury geometrycznej powierzchni*. Cz. 7, *Ocena chropowatości i falistości powierzchni*. „Mechanik", 5–6 (2005), s. 526–529.

[48] Antoszewski B.: *Influence of laser and plasma modification on surface properties of sliding and rubbing components*. Technical University of Kielce, 17, Kielce (1999), pp. 39–52.

[49] Gyk G., Etsion I.: *Testing piston rings with partial laser surface texturing for friction reduction*. Wear 216 (2006), pp. 792–796.

[50] Wan Yi, Xiong Dang-Sheng: *The effect of laser surface texturing on frictional performance of face seal*. Journal of Materials Processing Technology, 197 (2008), pp. 96–100.

[51] Antoszewski B., Radek N.: *Tribologiczne i technologiczne aspekty teksturowania par ślizgowych o powierzchniach płaskich.* „Tribologia, teoria i praktyka", 2 (2008), s. 25–33.

[52] Antoszewski B., Radek N., Tarelnik W.: *Mikroteksturowanie powierzchni ślizgowych par tarcia obróbką elektroerozyjną*. Zeszyty Naukowe Politechniki Świętokrzyskiej – „HERVICON 2008", Budowa i Eksploatacja Maszyn, 10 (2008), s. 231–238.

[53] Antoszewski B., Radek N.: *Technologia oraz cechy powierzchni teksturowanych metodą laserową i elektroerozyjną*. „Inżynieria Maszyn", R. 12, 4 (2009), s. 5–12.

[54] Antoszewski B., Radek N., Tarelnik W., Wajs E.: *Electro discharge and laser texturing of sliding face of mechanical seals*. IX International Conference HERVICON – Sumy, Ukraina, T. 3, 1 (2005), pp. 15–123.

[55] Radek N., Antoszewski B.: *Mikroteksturowanie powierzchni ślizgowych par tarcia technologią laserową i elektroerozyjną.* „Logistyka", 2 (2010), pp. 2149–2156.

[56] Radek N.: *Laserowe i elektroerozyjne teksturowanie par ślizgowych o powierzchniach płaskich.* „Mechanik", 11 (2010), s. 822–825.

[57] Kunda J., Broncek J., Hadzima B.: *Experimental access to invvestigation of tribocorrsive properties of mechanical parts surfaces.* Scientific basic of moder Technologies: Experience and Prospects, Ukraina, (2011), pp. 299–310.

[58] Broncek J., Vidiečan J., Dzimko M.: *Comparison of roughness measurement methods*. Zeszyty Naukowe Politechniki Świętokrzyskiej – IV Letnia Szkoła Inżynierii Powierzchni (2010), pp. 19–26.

[59] Arnold J., Muller G., Schneider H., Muller H.K., Hugel H.: *Production of micro structures in SiC slide rings with an excimer laser*. "Laser und Optoelektronik", 25 (1993), pp. 12–16.

[60] Etsion I.: *A laser surface textured hydrostatic mechanical seal sealing technology*. Sealing Technology, 3 (2003), pp. 6–10.

[61] Yu X.Q., He S.: *Frictional characteristics of mechanical seals with a laser textured seal face*. Journal of Materials Processing Technology, 129 (2002), pp. 463–466.

[62] Kovalchenko A., Ajayi A., Erdemir A., Fenske G., Etison I.: *The effect of laser surface texturing on transitions in lubrication regimes during unidirectional sliding contact.* Tribology International, 38 (2005), pp. 219–225.

[63] Erdemir A.: *Review of engineered tribological interfaces for improved boundary lubrication*. Tribology International, 38 (2005), pp. 249–256.

[64] Volchok A., Halperin G., Etsion I.: *The effect of surface regular microtopography on fretting fatigue life*. Wear 235 (2002), pp. 509–515.

[65] Miller K.J.: *Structural integrity – whose responsibility?,* 36th John Player Lecture, IMechE, Sheffield 2001, p. 24.

[66] Mindlin R.D., Deresiewicz H.: *Elastic spheres in contact under varying oblique forces.* ASME J. Appl. Mech., 75 (1953), pp. 327–344.

[67] Ciavarella M.: *The generalized Cattaneo partial slip plane contact problem*. I-Theory. Int. J. Solids Struct 35, 18 (1998), pp. 2349–2362.

[68] Menq C.H., Bielak J., Griffin J.H.: *The influence of microslip on vibratory response. A new microslip model.* Part I. Journal of Sound and Vibration 107, 2 (1986), pp. 279–293.

[69] Menq C.H., Bielak J., Griffin J.H.: *The infuence of microslip on vibratory response a new microslip model.* Part II, Journal of Sound and Vibration 107, 2 (1986), pp. 295–307.

[70] Tomlinson G.A.: *The rusting of steel surfaces in contact*. Proc. Roy. Soc. Lond. A 115, 1927, pp. 472–483.

[71] Tomlinson G.A., Thorpe P.L., Gough H.J.: *An Investigation of the Fretting Corrosion of Clossely Fitting Surfaces*. Proc. Inst. Mech. Eng., 141 (1939), pp. 223–249.

[72] Ruiz C., Chen K.C.: *An investigation of fatigue and fretting in a dovetail joint*. Experimental Mechanics, 24 (1984), pp. 208–217.

[73] Tritschler B., Forest B., Rieu J.: *Fretting corrosion of materials for orthopaedic implants: a study of a metal/polymer contact in an artificial physiological medium.* Tribol. Int., 32 (1999), pp. 587–596.

[74] Antoszewski B.: *Warstwy powierzchniowe z teksturą – kształtowanie wybranymi technologiami wiązkowymi oraz właściwości tribologiczne.* Wydawnictwo Politechniki Świętokrzyskiej, Kielce 2010.

[75] Antoszewski B.: *Problems of maintenance of sustainable technological systems.* [w:] *Improvement of the conditions of lubrication friction ties by laser textured lubrication*. Wydawnictwo PNTTE 2010, Tom 1, pp. 62–75.

[76] Antoszewski B.: *The formation of antiwear surface layers on elements of machine parts.* Zagadnienia Eksploatacji Maszyn, Vol. 44, 2 (2009), pp. 7–19.

[77] Antoszewski B.: *Production, properties and application of laser textured components*. "Logistyka" 6 (2009), pp. 88–100.

[78] Petru M., Novak O., Herák D., Simanjuntak S.: *Finite element method model of the mechanical behavior of Jatropha curcas L. seed under compression loading.* Journal homepage: www.elsevier.com/locate/issn/15375110, Biosystems Engineering, 111 (2012), pp. 412–421.

[79] Brezinová J., Guzanová A., Egri M.: *Change in properties of HVOF coatings under conditions of thermal cyclic loading.* Chemické listy, Vol. 106, No. S3 (2012), pp. 383–386.

[80] Romer G.R.B.E., Meijer J., Olde Benneker J.: *Process control of laser surface alloying.* Surface Engineering, 4 (1998), pp. 295–298.

[81] Wielage B., Steinhauser S., Pawłowski L., Smurov I., Covelli L.: *Laser treatment of vacuum plasma sprayed CoCrAlY alloy.* Surface Engineering, 5 (1998), pp. 391–394.

[82] Dini J.W.: *Laser surface modification offers promise for various coating processes and substrates.* Metal Finishing, October 1997, pp. 10–14.

[83] Khedkar J., Khanna A.S., Gupt K.M.: *Tribological behaviour of plasma and laser coated steels.* Wear, 205 (1998), pp. 220–227.